Manuel Rocha Lecture

Manuel Rocha (1913-1981) was honoured by the Portuguese Geotechnical Society with the establishment of the Lecture Series bearing his name in 1984.

Having completed the Civil Engineering Degree at the Technical University of Lisbon (1938) he did post-graduate training at MIT. He was the driving force behind the creation of the research team in Civil Engineering that would lead to the foundation of the National Laboratory for Civil Engineering (LNEC), in Lisbon. He was Head of LNEC from 1954 to 1974 and led it to the cutting edge of research in Civil Engineering.

His research work had great impact in the area of concrete dams and rock mechanics. He was the 1st President of the International Society for Rock Mechanics and organized its 1st Congress in Lisbon (1966). He did consultancy work in numerous countries. He was Honorary President of the Portuguese Geotechnical Society, having promoted with great commitment the cooperation between Portugal and Brazil in the area of Civil Engineering, and member of the National Academy of Sciences of the USA. Recognized as a brilliant researcher, scientist and professor, with a sharp, discerning intellect allied to a prodigious capacity for work and management, he was truly a man of many talents.

Prof. EDUARDO E. ALONSO, Civil Engineer (Madrid, 1969) and Ph.D. (Northwestern University, 1973), Full Professor at UPC, Barcelona in 1986 and member of the Royal Academy of Engineering of Spain in 1995. His areas of expertise include probability and statistics, unsaturated soil mechanics, rock mechanics, thermo-hydro-mechanical behaviour of soils, embankment dams and slope stability. He was awarded twice the Thomas Telford Medal, ICE, UK (1994 & 2006), the 2009 & 2010 Geotechnical Research Medals and the 2005 Crampton Prize; the José Torán Award (1995), Spanish Committee on Large Dams; the 2000 Narcis Monturiol Award, Generalitat de Catalunya and the Monterri Award (2014), Switzerland. He was the 2nd Coulomb Lecturer (2003), 11th Buchanan Lecturer (2003), 10th Sowers Lecturer (2007), 10th Arrigo Croce Lecturer (2011), 1st Heim Lecturer (2012) and 3rd Kezdi Lecturer (2013).

Soils and Rocks
v. 37, n. 1

Fracture Mechanics and Rockfill Dams

Eduardo E. Alonso

Abstract. Rockfill behavior is dominated by particle breakage, a phenomenon which is analyzed from the perspective offered by the subcritical propagation of cracks within individual particles. Propagation velocity depends on stress concentration in particles as well as on the ambient Relative Humidity (RH). RH controlled oedometer and triaxial tests are reviewed and constitutive models reproducing the main features of observed behavior are outlined. The relevant issue of size effects is then introduced and some rules and possibilities to account for these effects in practice have been given. The Distinct Element Method is also a powerful tool to investigate rockfill behavior. Recent developments are described. The model developed incorporates particle breakage, delayed effects and the action of water. In the final part two real cases are presented: the response of a high rockfill embankment against a four year long rainfall regime and the analysis of Beliche dam. The lecture closes by a general discussion of partial saturation in granular materials ranging from coarse granular aggregates, such as rockfill, to clayey soils in an attempt to provide an integrated overview of water effects in soils.

Keywords: rockfill, fracture mechanics, crack propagation, relative humidity, suction controlled testing, constitutive models, embankments, dams, case histories.

1. Motivation

The use of rockfill as a construction material goes back to early civilizations. An outstanding example is Sadd-el-Kafara dam (Fig. 1) built in Egypt in 2,600 B.C. (Schnitter, 1994). The dam, 14 m in height, had an impervious core protected by two rockfill shoulders, bounded by a masonry fabric. However, it was at the beginning of the 20th Century that the design of dams including rockfill was generalized. Two types were designed: either a zoned structure which integrates rockfill shoulders and some internal impervious core, or an entire rockfill resisting structure, made impervious by an upstream blanket.

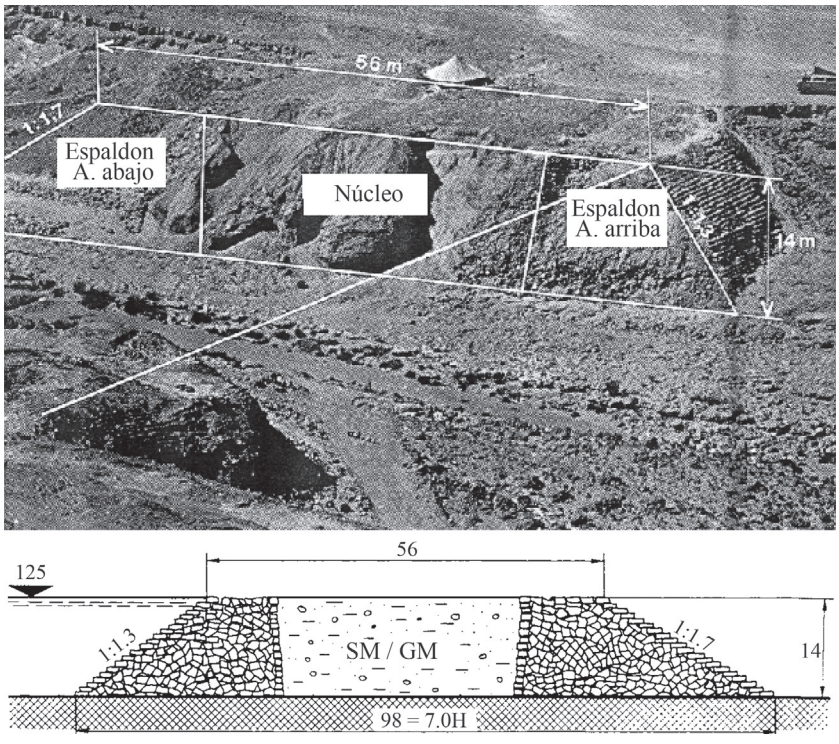

Figure 1 - Sadd-el-Kafara. Rockfill dam built in Egypt in 2600 b.C. (Schnitter, 1994). Following Casagrande classification, SM/GM describes the core material. SM: silty sand, GM: silty gravel. Dimensions in meters.

Eduardo E. Alonso, PhD, Professor of Geotechnical Engineering, Universidad Politécnica de Cataluña, Barcelona, Spain. E-mail: eduardo.alonso@upc.edu.
Invited Lecture, No discussion.

A modern example of a large dam (136 m in height) of triangular section made of compacted gravels and an upstream concrete face is Caracoles dam in the Argentinian Andes, close to the city of San Juan (Fig. 2). The construction material was, in this case, alluvial gravel compacted in layers (Fig. 3). This type of design is a popular one in the Andes mountain range, where there is often the possibility of building with river gravels, as clay is rather scarce.

A common design in Spain is the zoned rockfill dam: Imperviousness is guaranteed by the central compacted clay core and the stability of the entire structure is ensured by the large rockfill shoulders on both sides of the core. Most typically the rockfill comes from a quarry. Lechago dam, on the Pancrudo River, in the province of Teruel, is a recent example of this type of dams (Figs. 4-8). The quartzitic shale gravel (Figs. 7 and 8), used in the construction of this dam, has been analyzed in some detail in the last decade in the UPC Geotechnical Laboratory. Its behavior, which is described below, allowed also formulating elastoplastic constitutive models for these materials.

Figure 2 - Caracoles dam under construction (2007). San Juan, Argentina.

Figure 3 - Caracoles dam under construction (2007). San Juan, Argentina. Detail of the gravel fill.

In these large structures, settlements are observed, which may be rapid settlements (associated with the wetting of the upstream rockfill shoulder, for instance by the reservoir impoundment) or long-time settlements. Wetting

Figure 4 - Lechago dam, Teruel, Spain. Aerial view. February 2008.

Figure 5 - Lechago dam, Teruel, Spain. February 2008.

Figure 6 - Lechago dam. Core, filters and rockfill shoulders.

Figure 7 - Lechago dam. Detail of rockfill.

Figure 8 - Lechago dam. Outcrop of Cambric quartzitic shales quarried for rockfill material.

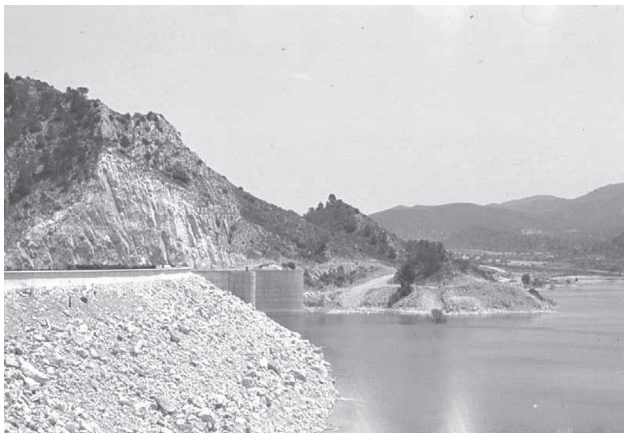

Figure 9 - Calanda dam, Teruel, Spain.

Figure 10 - Collapse settlements of rockfill in Calanda dam.

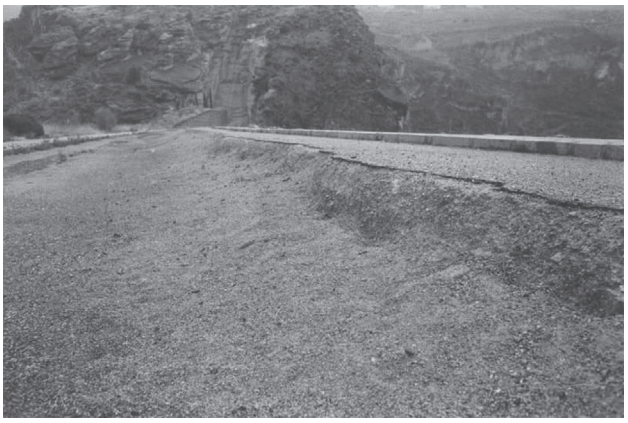

Figure 11 - Collapse settlements of rockfill in Martín Gonzalo dam, Córdoba, Spain.

induced settlement (collapse) is a consequence of the volumetric contraction experienced by the rockfill when the pores are filled with water. Figures 9 to 11 illustrate this phenomenon in two dams: Calanda dam, in Teruel, and Martín Gonzalo dam, in Córdoba. Figure 10 shows the effect of these deformations on the crest of the dam, and Fig. 11 shows the large settlement (in the upstream direction) observed in Martín Gonzalo dam, due to the wetting of the lower part of the resisting rockfill section. The upstream impervious membrane eventually fissured and reservoir water could freely saturate the rockfill.

Figure 12 illustrates a very significant phenomenon: settlement of the dam at different heights is well-correlated with rainfall. The figure shows that settlements concentrate in the periods of the year having the strongest rainfalls. In drier periods the settlement rate slows. In fact, the plot in Fig. 12 allows defining two types of settlements: a maintained, slow motion (which could be designated as creep) in dry periods, and a rapid settlement associated with intense rainfall (which wets the rockfill and results in collapse deformations). These collapse settlements disappear after the first three years of life of the dam. The reason for this behavior will be given later. Before, some basic discussion of

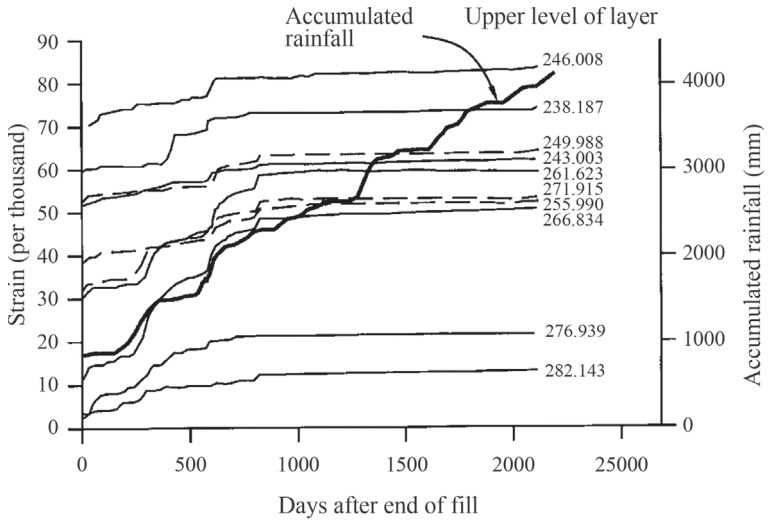

Figure 12 - Martín Gonzalo dam. Settlement of plates located at different heights in the axis of the dam maximum cross section and accumulated rainfall. Justo and Durand (2000).

the fundamentals of rockfill mechanics should be introduced.

The systematic measurement, for decades, of dam settlements after construction provides also interesting data on these structures (Sowers *et al.*, 1965; Sherard & Cooke, 1987; Marsal *et al.*, 1976). Figure 13 shows a summary of results published by different authors. Dams are classified in four groups. In ancient concrete face rockfill dams (CFRD) rock fragments were dumped without compaction. They suffer large settlements which may amount to more than 1% of dam height. However, modern CFRD dams, built with compacted rockfill exhibit much lower after compaction settlements. It was found that compacting these dams in layers, which is the common practice in earthfills, substantially reduced settlements. Data published by Sherard and Cooke (1987) show that, in compacted rockfill, postconstruction settlements remain in the order of 0.13% of dam height. Figure 13 shows similar results.

Settlements of dams made of alluvial gravels are also small. The reason goes back to the rounded nature of the particles and, also, to the often well graded materials found in alluvial deposits. Both characteristics limit the particle breakage.

Note also that recently built dams, made of compacted rockfill (Beliche in Portugal; Rivera de Gata in Spain) experienced large post-construction settlements. This behavior is explained by the type of rockfill. Fissile and brittle clayey rocks such as schists, shales, slates and grauwackes are prone to particle breakage which leads to comparatively larger settlements.

A common characteristic to all settlement curves in Fig. 13 is the long term record of settlements. Settlements are being measured after 20-30 years after the dam construction. Most of the curves in Fig. 13 may be described by a linear relationship between settlement and logarithm of time. Deformation does not stop although the settlement rate decreases continuously.

Post-construction settlements of rockfill dams may impair the dam safety or its operability. But, in general, no serious problems have been reported. Extreme cases such as Ataturk dam in Turkey (Cetin *et al.*, 2000), which exhausted the crest guard, five years after the dam commissioning, are rare events.

Rockfill embankments are frequently used in transport infrastructure. In high speed railway lines strict limits are applied to the expected total and differential settlements in order to guarantee the safe operation of trains.

Models for delayed deformations have been published by a few authors (Sowers *et al.*, 1965; Mesri & Castro, 1987; Charles, 1991; Soriano & Sánchez, 1999; Athanasiu *et al.*, 2005). Stress-strain models such as the hyperbolic Charles (1989) model and the visco-elastic formulation of Justo & Durand (2000) are phenomenological approximations to observed behavior. But a more detailed knowledge of basic physical phenomena at particle level may provide better models. This is the case for delayed deformations but also for the evaluation of strength, compressibility, water action and, in general, for a comprehensive constitutive behavior of these materials.

This paper starts by examining the breakage of particles as a fundamental mechanism to explain the behavior at a larger scale. Particle breakage, in turn, is explained by the propagation of cracks or fissures. Key aspects such as the velocity of crack propagation and the controlling factors (stress state, ambient Relative Humidity) will provide a satisfactory explanation to observations. They are also useful to conceive experimental programs aiming at developing constitutive models. A different approach, namely the capability of the Distinct Element Method, will be also described. At the end, it is the comparison between model

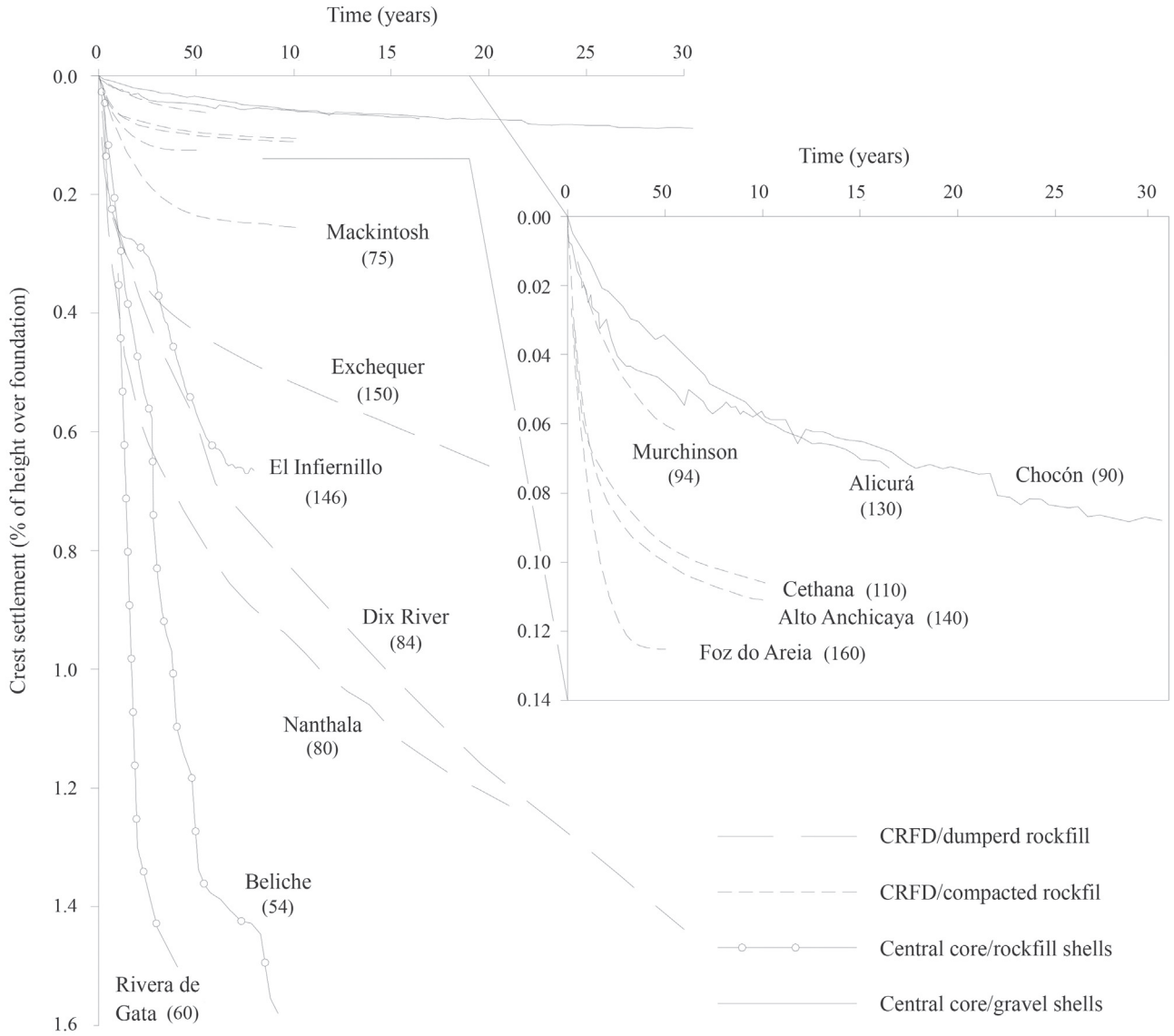

Figure 13 - Records of crest settlement of different types of rockfill dams built during the 20th century. Name (height in m) of the dam next to each curve. (data sources: Sherard & Cooke, 1987; Naylor *et al.*, 1997; Soriano *et al.*, 1992; Marsal *et al.*, 1976).

predictions and "in situ" behavior the necessary check to establish the practical applications of the ideas and models presented.

2. Background

2.1. Water induced collapse of rockfill

The action of water is fundamental to explain the development of settlements. Collapse of upstream rockfill shoulders, a phenomenon taking place during the first reservoir impoundment, is well known. The term "collapse" refers here to the increase of volumetric compression, at constant confining stress, induced by the action of water.

In parallel to field observations, laboratory tests in which samples of gravel were loaded and wetted at constant stress also experienced collapse deformations. Terzaghi (1960) attributed this behavior to particle breakage due to the weakening effect of water on the wetted rock.

Collapse settlements in dams and laboratory tests were reported by Sowers *et al.* (1965); Marsal (1973); Nobari & Duncan (1972). Figure 14a,b reproduces the results of oedometer tests performed on a crushed shale from Pyramid dam (Nobari & Duncan, 1972). Flooding samples initially dry, either at constant stress or at constant porosity, took the sample state to the compression curve for saturated conditions. This is a result formally identical to the behavior observed in partially saturated soils (Alonso *et al.*, 1987).

However, the deformation mechanisms of coarse granular aggregates and fine soils (fine sands and smaller particle size) should be fundamentally different. To illustrate this statement, Fig. 15 shows the variation of attractive cap-

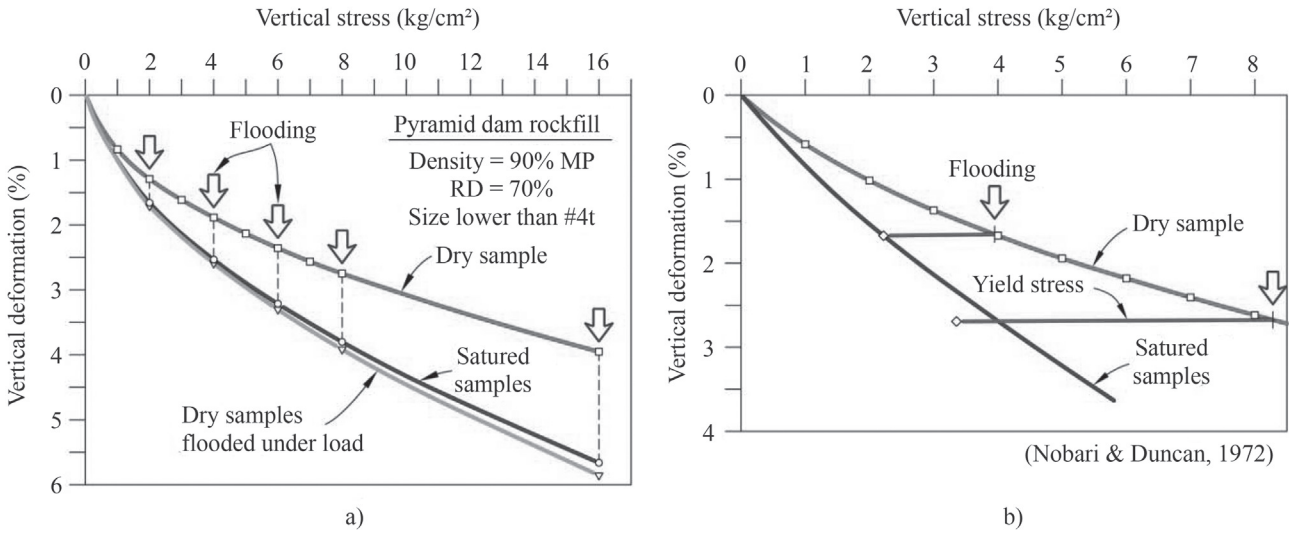

Figure 14 - Oedometer tests reported by Nobari & Duncan (1972) a) flooding at constant stress; b) flooding at constant volume.

illary force between two spherical particles when there is a water meniscus at the contact. The attractive force, F_w, was calculated following the theory of toroidal meniscus described in Gili (1988). In the four cases presented ("rockfill", diameter $D = 50$ cm; "gravel", $D = 10$ mm; medium sand, $D = 0.5$ mm and medium silt, $D = 0.01$ mm) the particle weight is used as an appropriate scale for the capillary force. For sizes larger than the size of small gravel, the particle weight is higher than the maximum capillary force

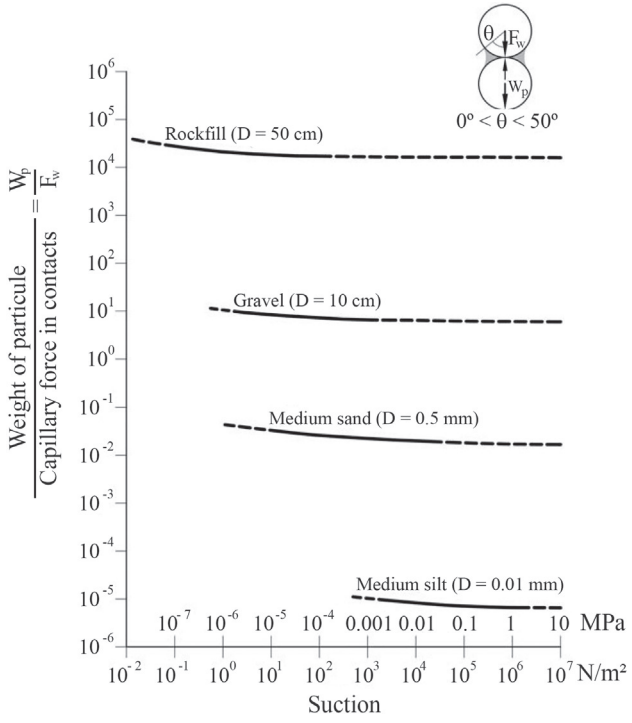

Figure 15 - Attraction capillary force in simple spherical cubic array.

in isolated menisci. Therefore, the internal capillary forces will tend to be negligible in coarse granular soils.

Figure 16 shows, in absolute terms, the capillary forces F_w. They are also represented as a normal stress across a reference plane which connects the contact points among spheres in a regular cubic array. The rapid reduction of the number of contacts when the particle size increases explain the low stress intensities calculated for the coarse aggregates. This is the case shown in Fig. 16 for the four materials considered in this example. It is concluded that capillary forces are not relevant to explain the effect of water on rockfill materials.

On the other hand compression tests on rock wedges in contact with surfaces of the same rock or against other material, performed by some authors (Sowers *et al.*, 1965; Marsal, 1973; Clements, 1981) suggest that contact failure is the fundamental mechanism explaining rockfill deformation and also explain water effects. Figure 17a shows a compression test of a rock wedge (vertex angle 169.1°) reported by Clements (1981). The effect of saturating the contact point, two hours after the application of the compression load, is to suddenly accelerate the deformation in a manner similar to observations in oedometer tests on samples of crushed greywacke and sandstone described by Sowers *et al.* (1965) (Fig. 17b).

These tests suggest that the deformation of the granular aggregate under the water action has to be explained, to a certain extent, as a result of the fracture of the rock matrix. These phenomena are revisited later.

2.2. Shear strength

The research carried out in the 60's and 70's of the 20th century clearly established the particle breakage as the dominant deformation mechanism of rockfill and gravels. Marsal (1973) and Hardin (1985) proposed breakage indi-

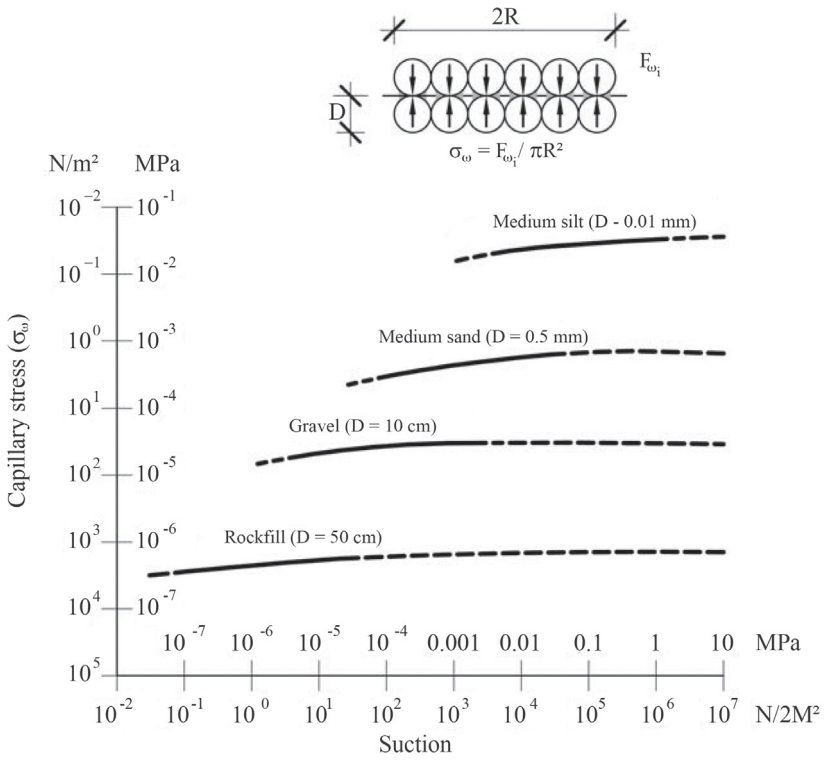

Figure 16 - Capillary attraction stress in a simple spherical cubic array.

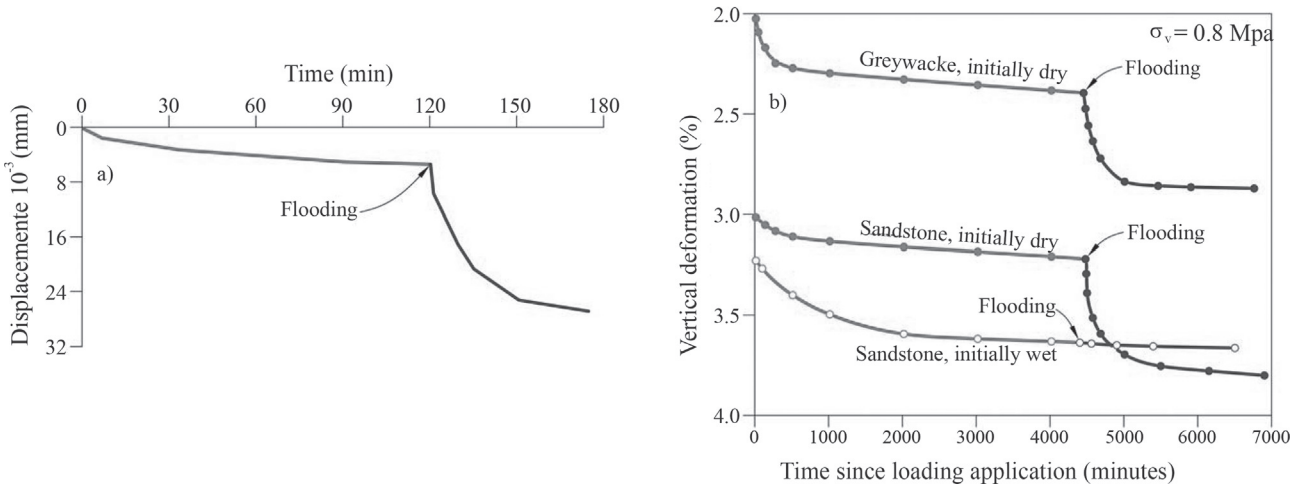

Figure 17 - a) Flooding test on a rock wedge (Clements, 1981); b) Effect of flooding the sample in oedometer tests of crushed rock under a constant vertical stress of 0.8 MPa (Sowers *et al.*, 1965). Oedometer diameter: 190 mm, sample height: 100 mm; maximum size of particles: 38 mm.

ces to quantify particle breakage. Large scale triaxial tests were also performed (Fumagalli, 1969; Marachi *et al.*, 1969; Marsal, 1973) in connection with the construction of large dams, especially in Mexico and the United States. The objective was to find the failure envelope, fundamental information to calculate the stability of dams. Charles & Watts (1980) stressed that the failure envelope was curved, especially for low confining stresses. This was one of the most relevant differences found when comparing soils and rockfill. For instance, the curved envelope:

$$\tau_f = A(\sigma)^b \quad (1)$$

where *A* and *b* are empirical constants, was proposed by De Mello (1977). The nonlinearity was attributed to the particle breakage during the entire stress path (confining and deviatoric stages).

Wetting tests at some instant during the performance of triaxial tests in large diameter samples (Veiga Pinto, 1983; Naylor *et al.*, 1986) also identified the partial collapse under the combined effect of average and deviatoric stress. This collapse resulted in a decrease of the strength of saturated samples, if compared with "dry" samples.

Figure 18 shows the strength envelope of the shale gravel used in the construction of Lechago dam. The gravel was tested in a suction controlled large diameter cell in the geotechnical laboratory of UPC. The attention given to suction (or, alternatively, Relative Humidity) is discussed below in more detail. The increase in RH of the sample resulted in a decrease of the sample shear strength.

The grain size distributions determined at the end of the triaxial tests, at different RH (Fig. 19), indicated that particle breakage (quantified by Hardin index) increases with RH. In the figure the breakage index is plotted in terms

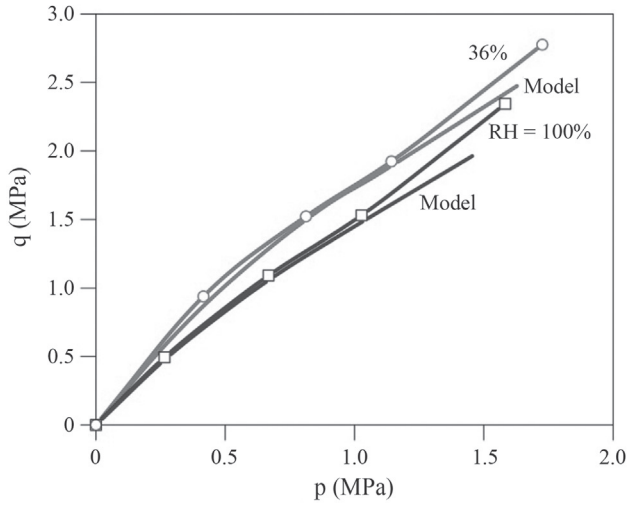

Figure 18 - Shear strength envelope of Pancrudo shale for RH = 36% and RH = 100% (Chávez, 2004).

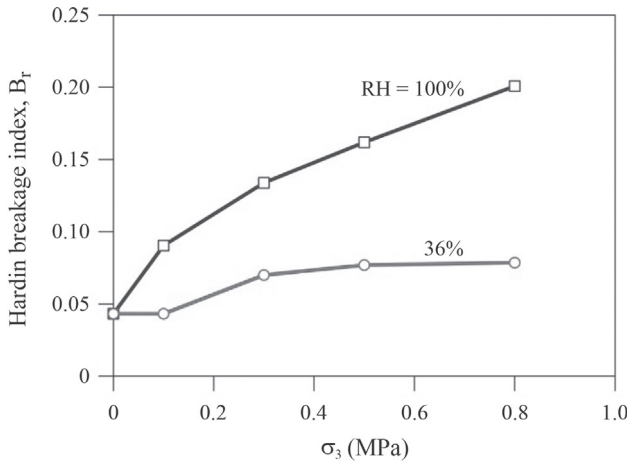

Figure 19 - Hardin breakage index determined in RH controlled triaxial tests on compacted Pancrudo shale (Chávez, 2004).

of the confining stress in the triaxial cell. The breakage index for $\sigma_3 = 0$ indicates the effect of compaction. Samples were in this case compacted under an energy equivalent to Standard Proctor.

The experimental and theoretical research on rockfill behavior came to standstill during the last two decades of the 20th century, perhaps as a consequence of the reduction of large hydraulic works in developed countries. The interest on these materials has resumed in recent years because of the need to develop prediction models which could compare with methods available for soils in general.

Probably, the best starting point to understand the accumulated experimental knowledge on rockfill behavior and, also, with the purpose of developing models of behavior at a macroscopic scale, is to examine in more detail the particle breakage phenomena.

2.3. Particle breakage

Figure 20a is a photograph of a sample of hard gravels of sandstone crushed and prepared to be tested in an oedometer cell having 30 cm in diameter and control over relative humidity. The gravel particles had a uniform size, which ranged 20 to 30 mm. The sample was not compacted initially. However, it was subjected to a cycle of loading reaching 2.3 MPa and later unloaded.

Figure 20b is a detail of the sample after the test. The breakage of particles is concentrated at the grain to grain contacts or else it divides de gravel into fragments of similar size. Very often the breakage plane crosses in a diametrical way the grain, whereas in other cases (Fig. 20c) the breakage is more complex.

Granular media have been analyzed extensively in the case of soils by the Distinct Element Method (DEM), following the pioneering work of Cundall & Strack (1979). It was found that the external stress applied to the assembly of grains is distributed into dominant forces that go through a series of well-defined chains of particles. Particles in these chains receive loadings concentrated at some contacts. The remaining particles, which constitute the granular media, are only slightly loaded and they contribute to stabilize the main loading chains. This interpretation explains the results of a DEM model, which includes capillary forces at the contacts, developed by Gili & Alonso (2002). Figure 21 show how, in an aggregate of spheres, the contact forces follow well-defined chains. Entire areas of the granular media remain unloaded.

Therefore, it is reasonable to start the discussion on the breakage of particles by considering a single particle loaded in a diametral way, as shown in Fig. 22. The breakage of particles observed in tests suggests that particles are broken due to crack propagation. In fact, the classic theory of Griffith, which explains the strength observed in rock samples, is based on a fracture mechanics concept, which attributed a fundamental role to the size of an initial defect

or discontinuity inside the rock matrix. This defect may be identified with an imperfect contact among crystals or else with pores or fissures of any nature.

Let us assume that particles are idealized as discs of diameter D and width B, having a defect or flaw in the central position, of size $2a_i$ in the direction of the two concentrated forces which act on opposite extremes of the diameter. The assumed loading on these particles is similar to the classic Brazilian Test. The diametral loading induces a uniform tensile stress perpendicular to the flaw.

These idealized assumptions lead to a Mode I (or pure traction mode) mode of failure in the theory of fracture

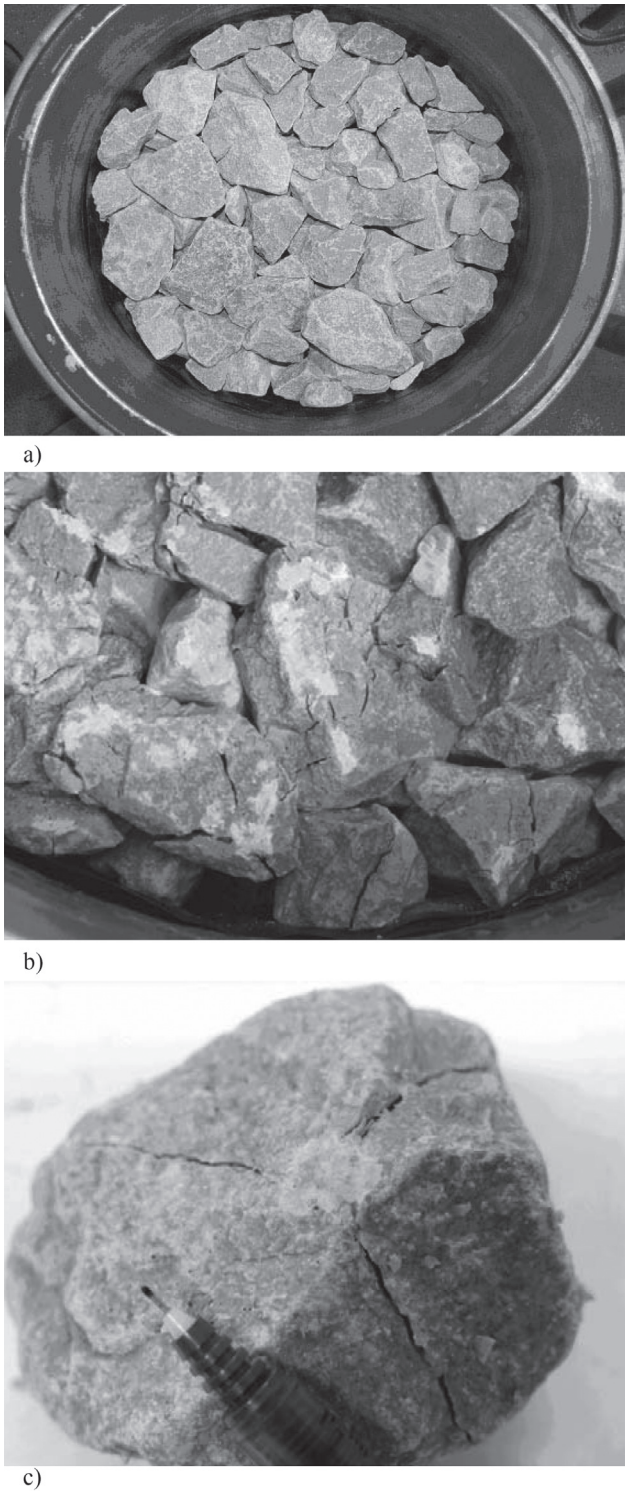

Figure 20 - a) Sample of hard crushed sandstone in an oedometer ell; b) Grain breakage after testing; c) Detail of a broken particle.

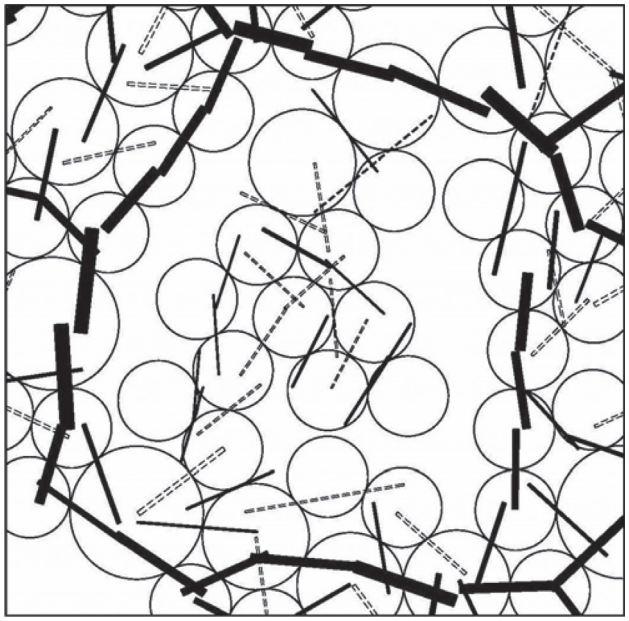

Figure 21 - Force chains in a loaded array of spheres. Thoroidal menisci exist at the grain to grain contacts. The thickness of plotted segments is proportional to the concentrated load. Discontinuous segments identify dominant capillary forces. (Gili & Alonso, 2002).

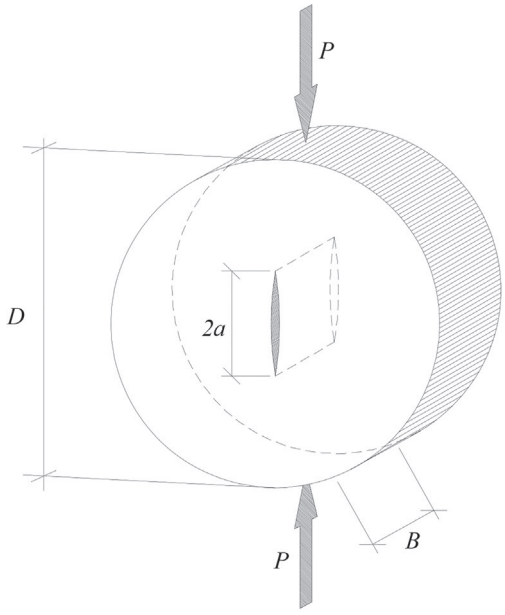

Figure 22 - Particle model for crack propagation (Oldecop & Alonso, 2007).

propagation of fracture mechanics. The implications of this model are explored below.

3. Crack Propagation in Particles

The propagation of the flaw in Tensile Mode 1 is associated in fracture mechanics to the concepts of toughness and stress intensity factor. The latter is defined as:

$$K_i = \beta_i \sigma_i^* \sqrt{\pi a_i} \quad (2)$$

where a_i is the initial length of the defect, β_i is a dimensionless factor that depends on (a_i/D) and σ_i^* is the tensile stress normal to the fracture plane if the particle is assumed to be intact. The σ_i^* stress should be related to the external "macro" stress on the granular aggregate. Therefore, σ_i^* increases with the external stress.

When K_i (i being an arbitrary crack) is lower than the material toughness, K_c, (units: MPa.m$^{1/2}$) the crack will propagate at a certain speed. This is known as the subcritical propagation of the crack. Crack propagation velocities, determined in experiments, have been collected in terms of (K/K_c) in Fig. 23. Experimental data may be approximated by a simple exponential relationship:

$$V = V_0 (K / K_c)^n \quad (3)$$

which is the dimensionless version of the equation originally proposed by Charles (1958). V_0 and n are model parameters. It should be stressed that Fig. 23 suggests that there is a velocity V_0 = 0.1 m/s for $K = K_c$. The exponent n changes with the prevailing suction. The information about the basalt, granite and marble, which is given in Fig. 23, is used to illustrate in Fig. 24 the approximate relationship between exponent n and RH. Data on synthetic quartz and glass suggests that n increases fast if the RH reaches low values. In other words, under conditions of extreme dryness, the propagation velocity of cracks tends to reach extremely low values.

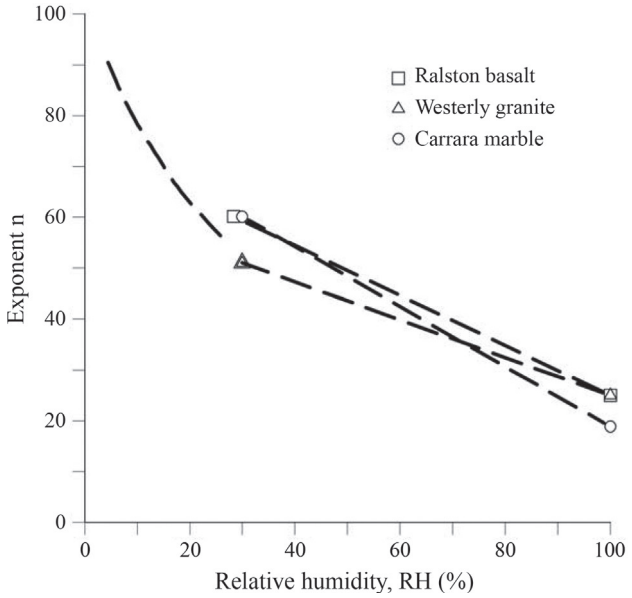

Figure 24 - Relationship between exponent n of Charles law and RH.

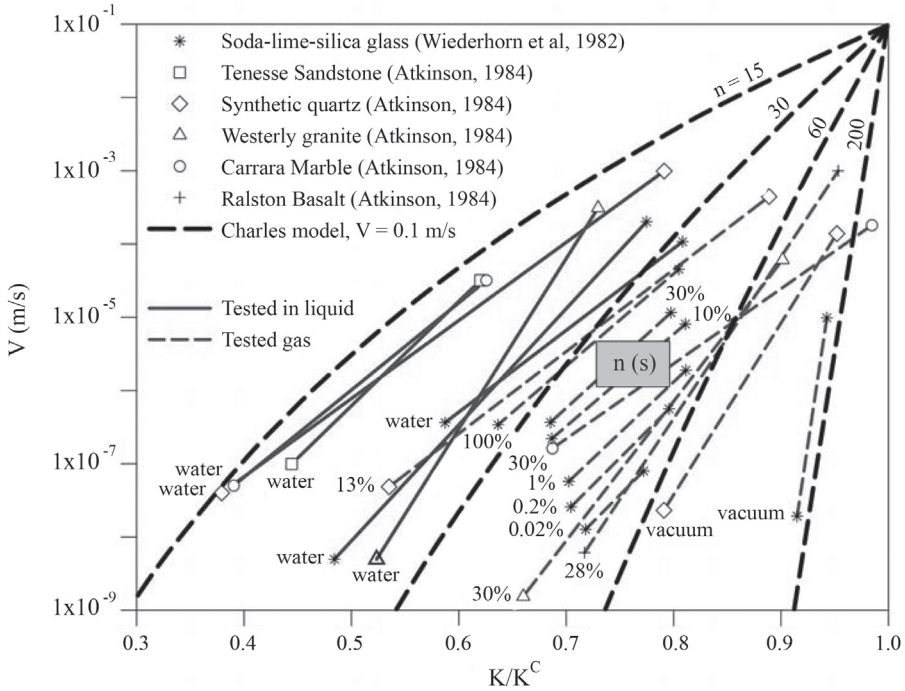

Figure 23 - Crack propagation velocities for different rocks, synthetic quartz and glass. Numbers (in %) indicate the RH of each experiment. Also shown are curves of Charles model (Oldecop & Alonso, 2007).

The velocity of propagation of cracks, V_i, may be expressed, taking into account Eqs. 2 and 3 as:

$$V_i = \frac{da_i}{dt} = A_i a_i^{n/2} \quad (4)$$

where

$$A_i = V_0 \left(\frac{\beta_i \sigma_i^* \sqrt{\pi}}{K_c} \right) \quad (5)$$

Equation 4 may be integrated if A_i is assumed to be constant, an approximation that is justified in Oldecop & Alonso (2007). Bearing in mind that the values of n are high (20-200), the failure time of the particle is given by:

$$t_i^b = \frac{2}{n-2} \frac{a_{0i}}{v_{0i}} \quad (6)$$

where

$$V_{0i} = V_0 \left(\frac{\beta_i \sigma_i^* \sqrt{\pi a_{0i}}}{K_c} \right)^n \quad (7)$$

is the velocity of propagation of the crack of length a_{0i}.

Equation 6 is plotted in Fig. 25 for the following set of parameters: $D = 500$ mm, $V_0 = 0.1$ m/s (taken from Fig. 23), $s = 7$ MPa and $K_c = 1$ MPaξm$^{0.5}$. The plot shows the failure time for different average lengths of initial defects and for the variable RH. The average relationship between n and the RH was taken from Fig. 24.

The plot shows what can be expected in the wetting phase (increasing RH): a significant reduction (of several orders of magnitude) of the breakage time. Breakage times of many years change into a few seconds. In practice this phenomenon is equivalent to a sudden failure if the entire granular assembly is considered. The macroscopic observation will be a sudden deformation (typically volumetric compressions or collapse).

For a given rock type (characterized by K_c and to a certain extent by a_{0i}) and a given particle size the failure time is also very sensitive to the stress applied, due to the high value of exponent n in Eq. 7. Therefore, an increment of σ will lead to the breakage of some grains and, as a consequence, it will induce an immediate deformation, even if the initial granular structure is kinematically "blocked".

An additional important aspect is that stressed fissures always increase in size, even if the crack propagation rate is very low. Therefore, at the scale of the rockfill in the field, creep deformations will always be present.

The information provided by experimental data (Fig. 23) can be synthesized in a conceptual model, which is plotted in Fig. 26.

The plot shows, again, the relationship between the velocity of propagation of a fissure and the stress intensity factor K. The velocity becomes infinite when K reaches the value of rock toughness K_c. The velocity depends also on the RH of the environment where the experiment is performed. If RH increases (which implies an increase in vapor concentration) so does the velocity of propagation. This effect is explained if the chemical reactions occurring at the tip of the crack are examined. The water acts as a corrosive agent of these reactions. The higher the energy of the water (increasing RH, lower suction), the higher the corrosive effect, and thus the velocity of fracture propagation. For every RH there is a threshold K below which there is no propagation (this threshold value is indicated as K_0 in Fig. 26). Therefore for a given RH, the values for K that lead to a given velocity of fissure progression are limited between K_0 and K_c.

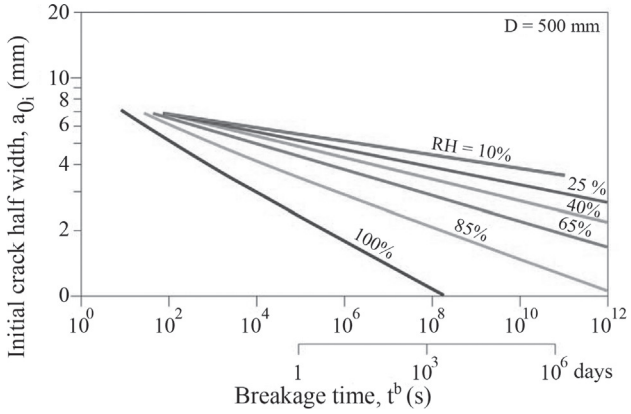

Figure 25 - Failure times for different initial crack lengths and different RH.

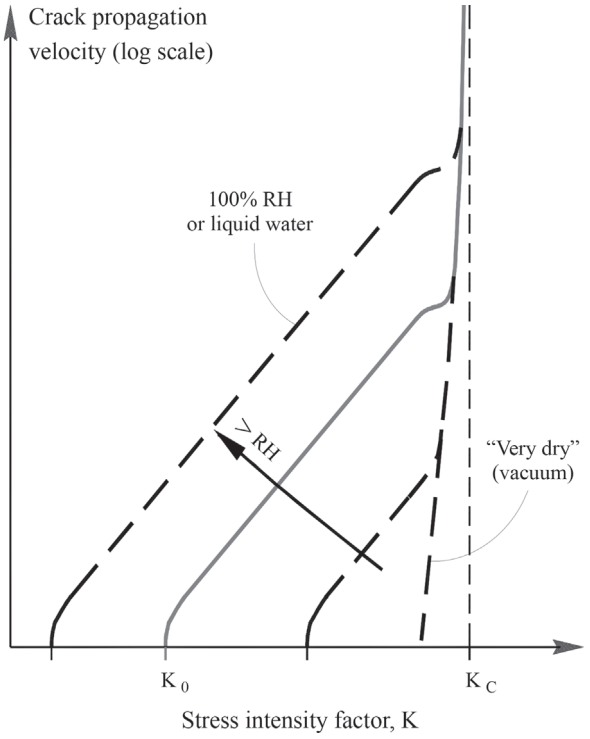

Figure 26 - Conceptual relationship between crack propagation velocity, stress intensity factor and Relative Humidity.

In a granular medium subjected to stress (rockfill dam) there will be a large number of loaded particles. Each of them will correspond to a value of K in the abscissas axis of Fig. 26. Given a RH, three different scenarios can be distinguished: fissures that do not propagate (region I: $K < K_0$), fissures which propagate at an increasing velocity with K (region II: $K_0 < K < K_c$), fissures that have already reached their maximum propagation velocity and the particle is broken (region III: $K = K_c$).

An increase in stress at constant RH will imply that several values of K will reach K_c. There will be a breakage of particles and the reorganization of the granular structure of the sample will be externally perceived as an increase of deformation. Moreover, the systematic increase of all the values of K implies an increase of the velocity of propagation and thus a further increase of particle breakage. In other words, there will be an increase of the deformation velocity of the granular medium.

The effect of an increase in RH is similar. The increase in the breakage velocity in all propagating fissures will lead to some breakage of grains, which will again result in volumetric contractions. Non active particle will become active and break in the future.

The perception of rapid settlement or collapse, when rockfill is wetted, is therefore the result of a series of internal breakages and the subsequent reorganization of the granular structure. Since RH plays a significant role in the breakage of particles, the next logical step is to perform suction-controlled experiments (total suction is involved, because total suction and RH are related through the psychrometric relationship).

4. Suction Controlled Oedometer and Triaxial Tests

4.1. Oedometer tests and constitutive modelling

Oldecop & Alonso (2001, 2007) described the results of large diameter (30 cm) suction controlled oedometer tests. The cell was described by Oldecop & Alonso (2004). Figure 27 shows the scheme of the test and the oedometer cell developed. Figure 28 shows the 30 cm diameter cell built. The experimental work performed confirmed the fundamental role of water. Figure 29 reproduces some results. The tested material was the Pancrudo shale used in Lechago dam, compacted to Standard Proctor energy.

The evolution of settlements with time for two RH (50% and 100%) and several confining stresses is consistent with the conceptual model of crack propagation in particles. In fact every load increment results in an acceleration of deformations. In a few minutes the deformation vs. time (log scale) curves exhibit a stationary creep. The slope of these stationary curves,

$$\lambda^t = \frac{d\varepsilon}{d(\ln t)} \qquad (8)$$

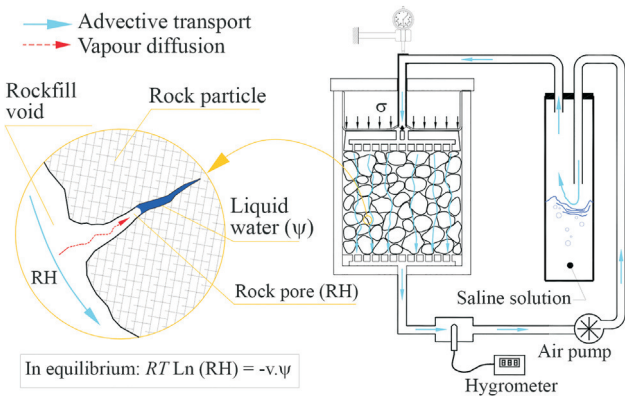

Figure 27 - Scheme of a suction controlled oedometer apparatus (Oldecop & Alonso, 2004).

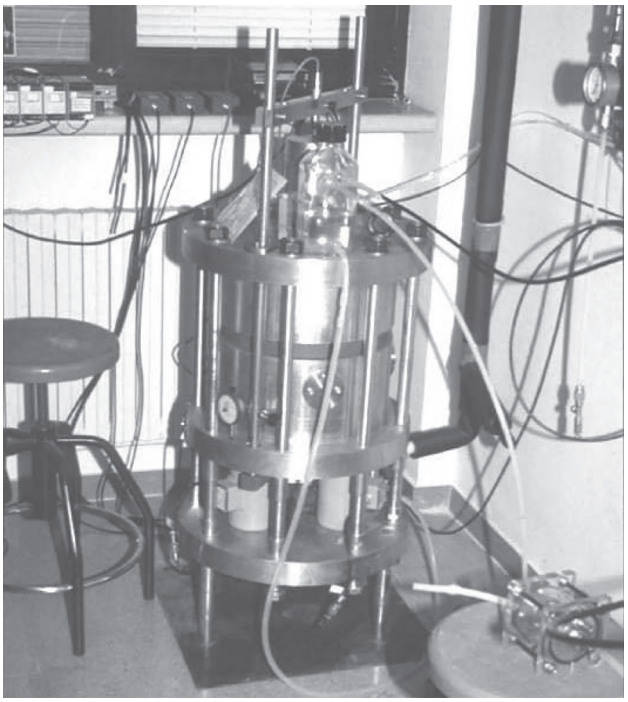

Figure 28 - Oedometer equipment with suction control developed by the geotechnical Laboratory of UPC.

becomes constant in time and increases with the applied stress. Suction reduction (wetting) leads also to an increase of the delayed compressibility index (Fig. 29).

Figure 30 shows that, for a limited range of stresses (say from 0 to 1.5 MPa) the delayed compressibility index may be described by the following expression:

$$\lambda^t = \mu p \left(1 - \beta \ln \frac{s + p_{atm}}{p_{atm}}\right) \qquad (9)$$

which shows the effect of confining stress, p, and suction, s. p_{atm} is the atmospheric pressure and (μ, β) are model parameters.

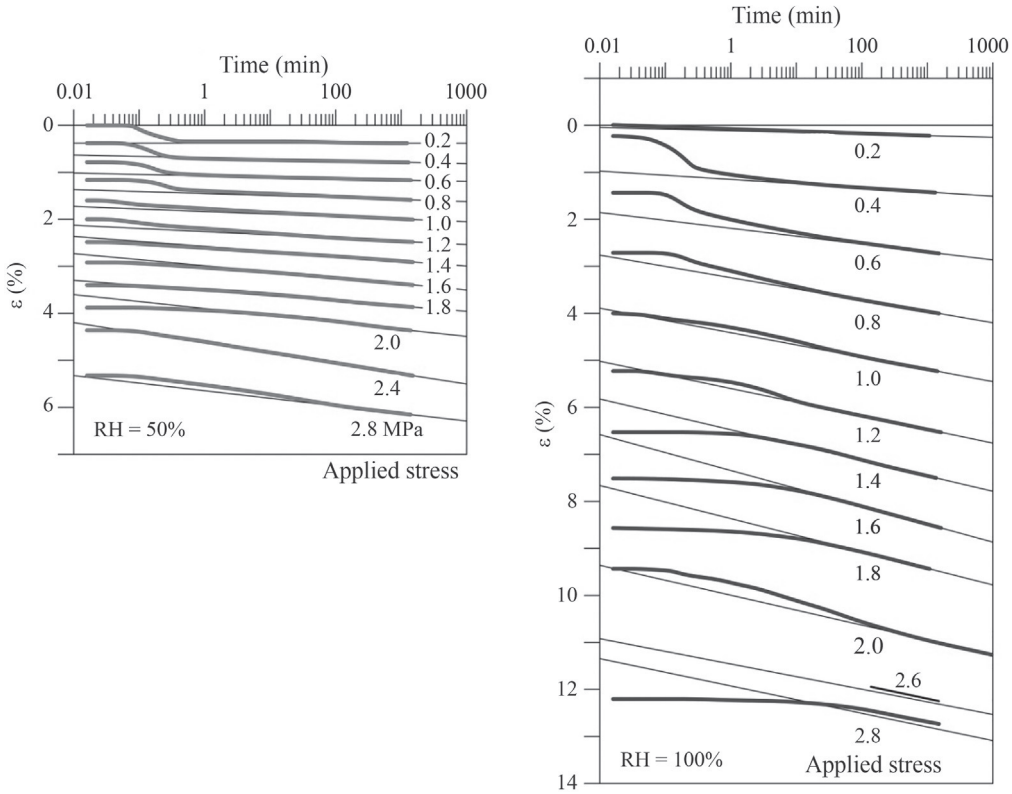

Figure 29 - Time -deformation records for oedometer tests on compacted Pancrudo shales at two different RH (50% and 100%) (Oldecop & Alonso 2007).

If deformations are selected at some particular time, stress-deformation relationships may be plotted for a stress and suction path applied to the sample. This is the case of Fig. 31 which shows the compressibility of compacted Pancrudo shale for a wide range of applied suctions and vertical stresses. The plot indicates that the compressibility reduces when suction increases, the collapse phenomena and the linear relationship between stress and deformation (natural scale) in a deformation range reasonably high (0-8%). Moreover, for stresses lower than a given threshold (around 0.2 MPa), compression behavior seems to be independent of applied suction (*i.e.*, independent from water content). This observation is consistent with the idea of a threshold of the stress intensity factor (K_0) described previously. Oldecop & Alonso (2003) identified and interpreted these features and they proposed an elasto plastic model to describe this behavior. The model could be justified physically by the crack propagation phenomena already described.

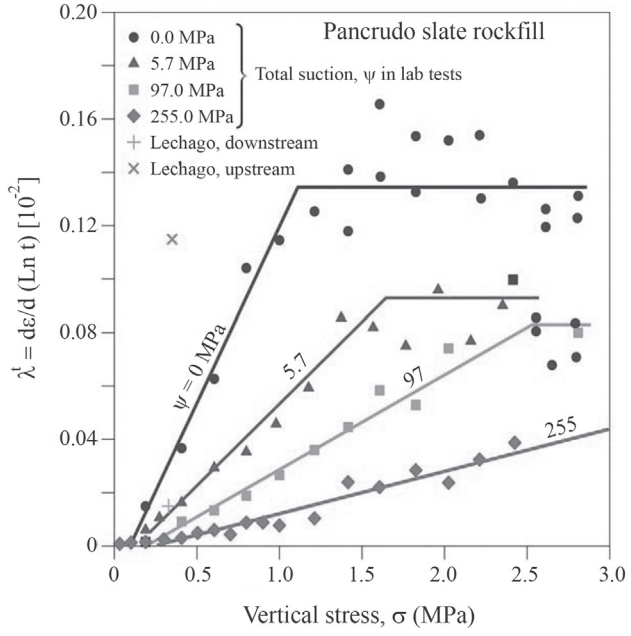

Figure 30 - Delayed compressibility index for Pancrudo shale. Effect of confining stress and applied suction (Oldecop & Alonso, 2007).

Compression curves in Fig. 31 are similar to the behavior of a "standard" unsaturated soil. Alonso (2006) discussed the similarities and differences in behavior between a compacted rockfill and a partially saturated soil.

It can be shown that the experimental volumetric behavior illustrated in Fig. 32 may be described by a strain hardening constitutive model (Oldecop & Alonso, 2001, 2003). The yield locus in a vertical stress-suction plane is defined by the equation:

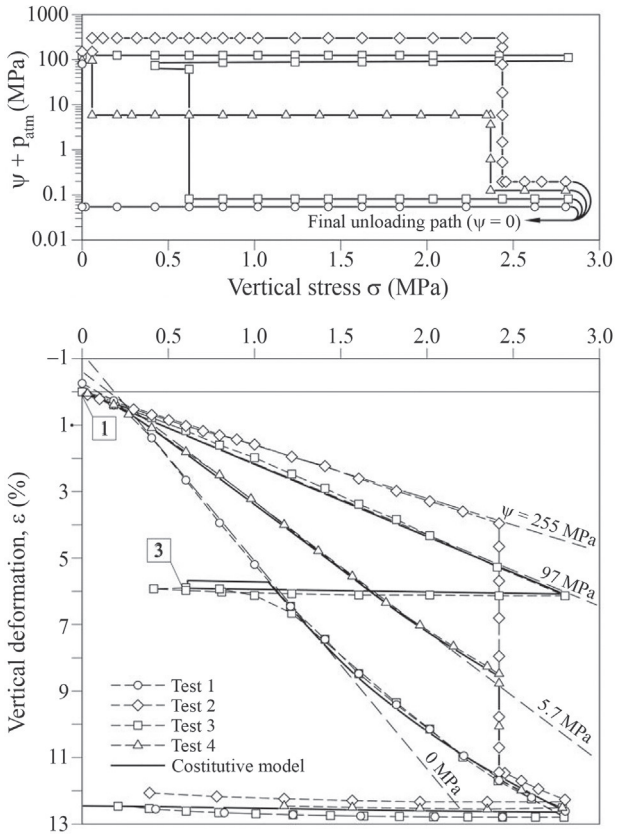

Figure 31 - Results of a series of oedometer tests on compacted Pancrudo shale. a) Stress paths; b) Stress-strain curves. Also indicated are model predictions (Oldecop & Alonso, 2003).

$$F(\sigma, \psi) = \sigma\left[\lambda(\psi) - \kappa\right] - \sigma_y\left[\lambda(\psi) - \lambda^i\right] - \sigma_0^*\left(\lambda^i - \kappa\right) = 0 \quad (10)$$

where the suction-dependent compressibility index is given by

$$\lambda(\psi) = \lambda_0 - \alpha_\psi \ln\frac{\psi + p_{atm}}{p_{atm}} \quad (11)$$

where σ_0^* is the hardening parameter, λ_0 is the saturated compressibility, λ^i compressibility for a very dry state, σ_y is the stress limit for particle re-arrangement and α_ψ is a parameter describing the increase of stiffness with suction.

Equation 10 is similar to the "Loading Collapse", LC, yield function defined for unsaturated soils (Alonso *et al.*, 1990). A main conceptual difference is that suction, in the case of rockfill has no any capillary stress interpretation. Equation 10 has been plotted in Fig. 32 for an increasing deformation. Also indicated in the figure are some frontiers which define the transition of deformation mechanisms in the manner described by McDowell & Bolton (1998): the transition from particle rearrangement (PR) and Clastic Yielding (CY) and the transition between Clastic Yielding and Clastic Hardening (CR).

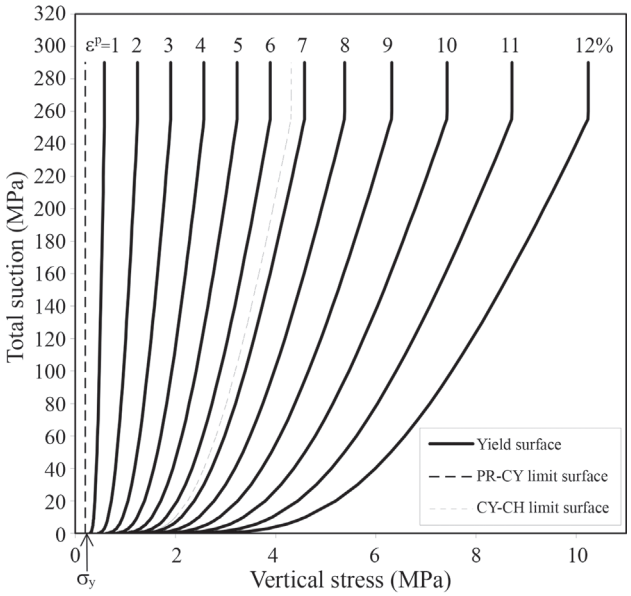

Figure 32 - Yielding (LC) curves for increasing values of plastic volumetric strain.

Figure 33 illustrates the capability of the model to simulate a stress path involving loading, unloading, wetting and reloading of an oedometer test on compacted gravel.

The model described was generalized to isotropic stress states, triaxial states (by adopting elliptical yield curves in the deviatoric plane) and, finally to general stress states. It was also introduced in the finite element code CODE_BRIGHT as the "Rockfill Model". Examples of application of this model to the analysis of a rockfill embankment and a zoned earth and rockfill dam are given later. In

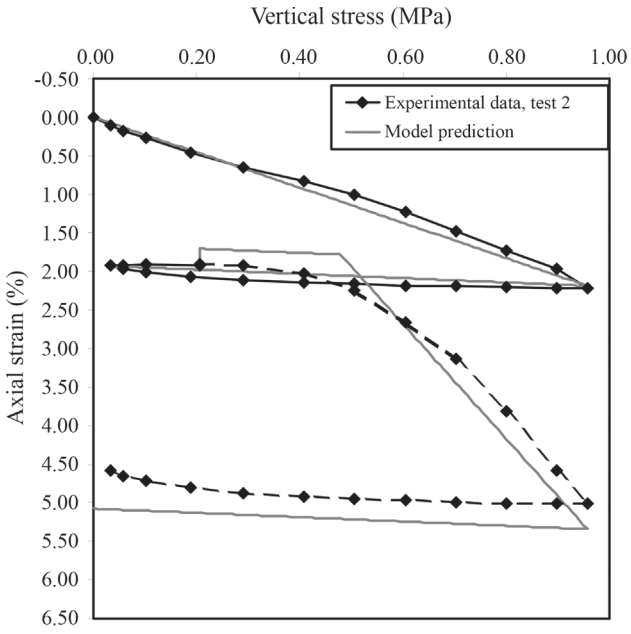

Figure 33 - Comparison of measured response of Pancrudo shale in an oedometer test and model predictions.

the remaining of this section the response of the rockfill under triaxial stress states will be briefly presented.

4.2. Triaxial stress states

Suction controlled triaxial tests were performed in the equipment described in Fig. 34 (Chávez *et al.*, 2009) with the purpose of investigating yielding and plastic flow behavior. One procedure to investigate the shape of yield loci was described by Poorooshasb *et al.* (1966) (Fig. 35). The shape of the yield locus and vectors of plastic strain increment are given in the figure. They suggest that hardening of rockfill is due to a combination of volumetric and deviatoric plastic strains. Plasticity is non-associated. Chávez & Alonso (2003) developed a full elasto-plastic model which was in part based on previous developments concerning the compressible behavior of rockfill identified in oedometer tests. The model incorporated a set of experimental observations:

- Critical state is found at the end of shearing paths. Suction contributes to maintaining higher void ratios if compared with saturated tests. Ultimate stress ratio increases with suction.
- The critical deviatoric stress is a nonlinear function of isotropic confining stress
- Two yield surfaces are proposed: a deviatoric one (q/p = constant) and an isotropic or "cap" surface (Fig. 36).
- Deviatoric behavior is described by means of a hyperbolic hardening rule which may also reproduce softening. Hardening is described by means of an effective plastic work and a deviatoric plastic strain. The effective plastic work is a procedure to account for the degradation of the material due to particle breakage.
- The plastic potential is based on a modified version of a Rowe dilatancy rule.

Figure 37 compares the model behavior with experimental results.

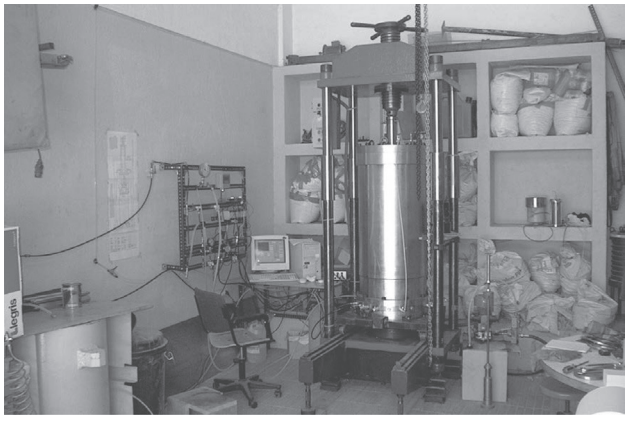

Figure 34 - Suction controlled large diameter triaxial cell of UPC geotechnical Laboratory.

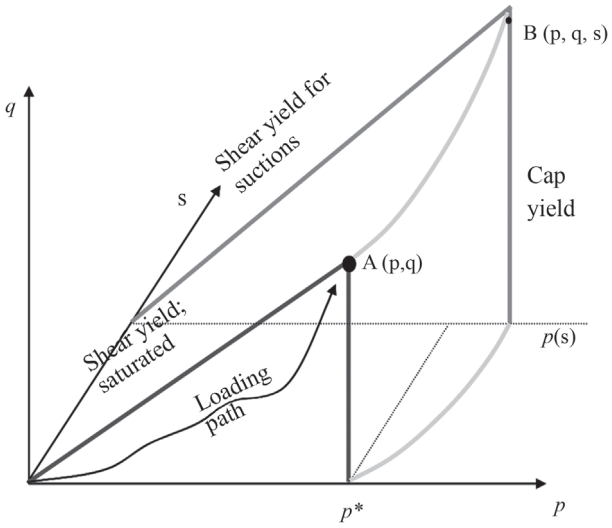

Figure 36 - Yield surfaces in Chávez & Alonso (2003) model.

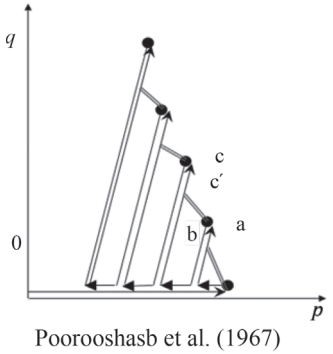

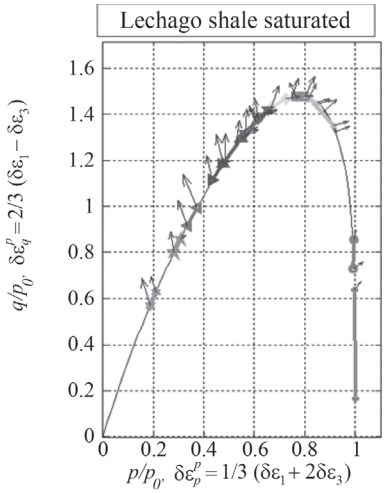

Figure 35 - Protocol for the investigation of yielding function shape in the deviatoric plane and yield locus for Pancrudo shale as reported by Chávez (2004).

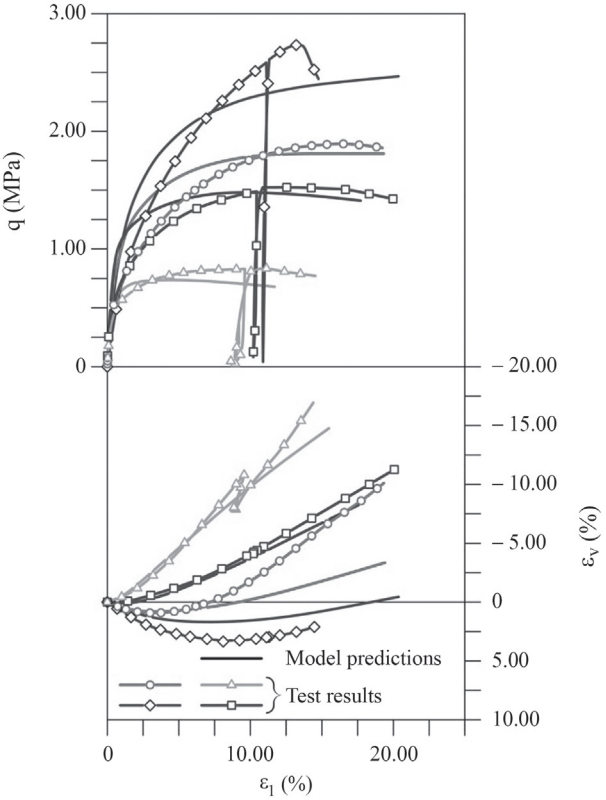

Figure 37 - Triaxial tests on Pancrudo shale at a RH = 36% and model predictions (Chávez & Alonso, 2003).

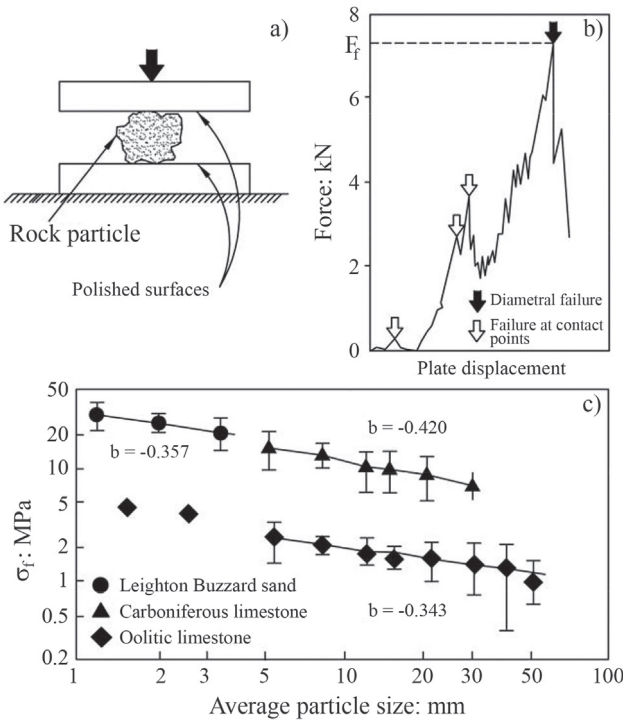

Figure 38 - Test on rock particles (McDowell & Bolton, 1998 quoting Lee, 1992): a) Test layout for determining the tensile strength of rock fragments. b) Typical load-displacement record. c) Variation of average tensile strength with particle size

5. Scale effects

Experimental evidence indicates that rock strength decreases as sample size increases. A common explanation is that the probability of finding a largest crack or defect in a critical direction increases with sample size.

In experiments which reproduce Type I (tensile) stress conditions, strength is shown to decrease with sample size. Figure 38 shows some results published by Lee (1992). The figure shows the type of test (an irregular particle is loaded along a diameter by means of two parallel polished rigid plates) and the relationships load-displacement. Local failures are initially detected at the grain-plate contacts, before a global diametric failure takes place. Tensile stresses on the diametric plane may be approximated from the well-known expression for the Brazilian test. This stress may be then compared with the average particle size of the sample. The results for three different lithologies are given in Fig. 38c.

The expression:

$$\sigma_f \approx d^{\alpha} \tag{12}$$

where σ_f is the tensile strength and α is a coefficient varying between -0.34 y -0.42, reproduces experimental results.

Fracture mechanics provides also an explanation for the experimental results. Cracks propagate when the stress intensity factor K reaches the material toughness K_c. Therefore, following Eq. 2 the tensile strength which leads to the propagation of the fissure is:

$$\sigma_f = \frac{K_c}{\beta\sqrt{\pi a_i}} \sim a_i^{-0.5} \tag{13}$$

It may be argued that the largest the particle diameter, the largest the initial defect in statistical terms. Therefore, the particle size defines the maximum size of a defect, critically oriented, capable of initiating a crack propagation leading to failure. Then,

$$\sigma_f \sim d^{-0.5} \tag{14}$$

Coefficients α in Eq. 1, experimentally determined by Lee (1992), are close to the theoretical coefficient given by Eq. 14 (-0.5). Consider now the relationship between the external stress, σ_{ext}, and the tensile stress, σ_t. In a particle loaded in the direction of a diameter, the concentrated load, P, is proportional to the tensile stress and the square of the diameter,

$$P \sim \sigma_t d^2 \tag{15}$$

and, in view of Eq. 14:

$$P \sim d^{-0.5} d^2 \sim d^{3/2} \tag{16}$$

will be the failure load.

In a regular arrangement of particles (assumed to be spheres) (Fig. 39), equilibrium will require:

$$\sigma_{ext} 1^2 = \sum P = P \frac{1}{d} \frac{1}{d} = \frac{P}{d^2} \quad (17)$$

Therefore,

$$P = d^2 \sigma_{ext} \quad (18)$$

and, Eq. 16 will lead to:

$$d^2 \sigma_{ext} \sim d^{3/2} \quad (19)$$

and

$$\sigma_{ext} \sim d^{-0.5} \quad (20)$$

In other words, the external stress able to break particles of diameter d is inversely proportional to $d^{0.5}$. The largest the particles, the easier its breakage for a given external stress. If, instead of Eq. 13, the starting point is Eq. 12, experimentally derived, Eq. 20 will transform into:

$$\sigma_{ext} \sim d^{-\alpha} \quad (21)$$

where α varies between 0.3 and 0.5.

Therefore, the mechanical properties of rockfill, which are controlled by particle breakage, will experience a scale effect, associated with to particle size. Eqs. 20 or 21 are useful to estimate the scale effect.

Consider rockfill compressibility. Due to the linear stress-strain relationship for an extended deformation range (Fig. 31), the compressibility coefficient, for a given suction, may be simply defined as:

$$\lambda \sim \frac{\Delta \varepsilon}{\Delta \sigma} \quad (22)$$

and, taking Eq. 21 into account:

$$\lambda \sim d^{\alpha} \quad (23)$$

If the compressibility of two granular aggregates, defined by diameters d and d_0, is compared:

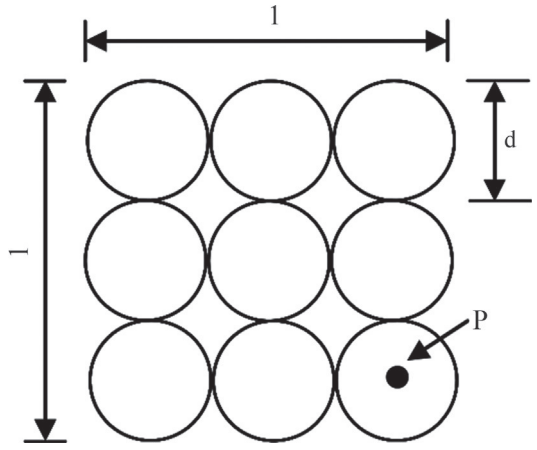

Figure 39 -.Simple arrangement of spheres. Plan view.

$$\lambda^d = \lambda^{d_0} \left(\frac{d}{d_0} \right)^{\alpha} \quad (24)$$

Figure 40 shows experimental results of gravel compressibility. Samples of hard crushed limestone of uniform size (40-30 mm, 30-20 mm, 25-20 mm and 20-10 mm) were tested in a 30 cm diameter odometer test (Ortega, 2008). The linear coefficient of compressibility for saturated conditions is plotted in terms of the maximum grain diameter. Two packing states were tested: a loose sample ($e_0 = 0.947$) and a dense state ($e_0 = 0.502$). Figure 40b shows the scaled compressibility, following Eq. 24 and taking d_0 as the maximum size of the simple grains. The plot shows that the exponent $\alpha = 0.5$ fits almost perfectly well the results for $e_0 = 0.947$. The dense aggregate ($e_0 = 0.502$) requires a value $\alpha = 0.3$ for a good fit of experiments. The scaling law is therefore affected y the degree of compaction.

Frossard (2009) discusses scale effects in a similar manner. When shear strength is considered (Eq. 1), the scaling law should be applied to the shear strength, τ_f, and the confining stress, σ. Then:

$$\frac{\tau_f}{\left(\frac{d}{d_0} \right)^{-\alpha}} = A_0 \sqrt[b]{\frac{\sigma}{\left(\frac{d}{d_0} \right)^{-\alpha}}} \quad (25)$$

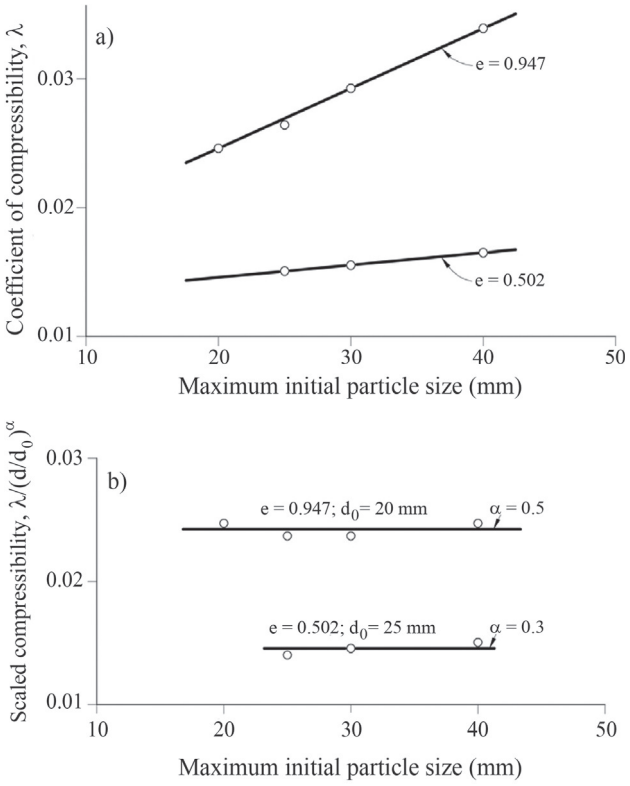

Figure 40 - a) Compressibility coefficient of uniform limestone gravels in terms of the maximum particle size (Ortega, 2008). b) Compressibility corrected for scale effects.

and:

$$\tau_f = A_0 \sigma^b \left(\frac{d}{d_0} \right)^{\alpha(1-b)} \quad (26)$$

This relationship provides the shear strength of a rockfill having a particle size d if the strength envelope of a rockfill having a particle size d_0 ($\tau_{f0} = A_0 \sigma^b$) is known.

The discussion on scale effects becomes more complex if non uniform grain size distributions are considered. In this case some of the assumptions leading to the preceding relationships are not satisfied, even in an approximate manner. In addition, a full characterization of the stress-strain behavior of a rockfill requires a number of parameters, defined in the adopted constitutive model. Scale effects do not affect only compressibility and shear strength.

However, if a given constitutive model is adopted, there is a possibility of testing different grain size distributions and constitutive parameters could be related to some indices describing grain size distribution. This approach was followed by Ramon *et al.* (2008), when they tested Pancrudo shale gravels, defined in Fig. 41. Three of the grain size distributions are characterized by a common D_{50} and a variable content of fines. The elastoplastic constitutive model adopted has been outlined above.

It was found that the best parameter identifying the grain size distribution was in this case the index D_{max}/D_{min}. Compressibility parameter λ_0^d decreases continuously when D_{max}/D_{min} increases (Fig. 42a). Parameter χ (Fig. 42b) which describes collapse intensity seems to decrease with D_{max}/D_{min} (Fig. 42b). The elastic compressibility parameter, κ, does not change with grain size distribution in this particular case. The delayed compressibility index, λ^t, maintains a constant relationship with the compressibility index, λ, and this result defines the scale effect for λ^t.

Scale effect is an interesting research topic, very relevant in practice, due to the limitations of laboratory testing. This topic will be examined again when introducing the capabilities of the Distinct Element Method to analyze rockfill behavior.

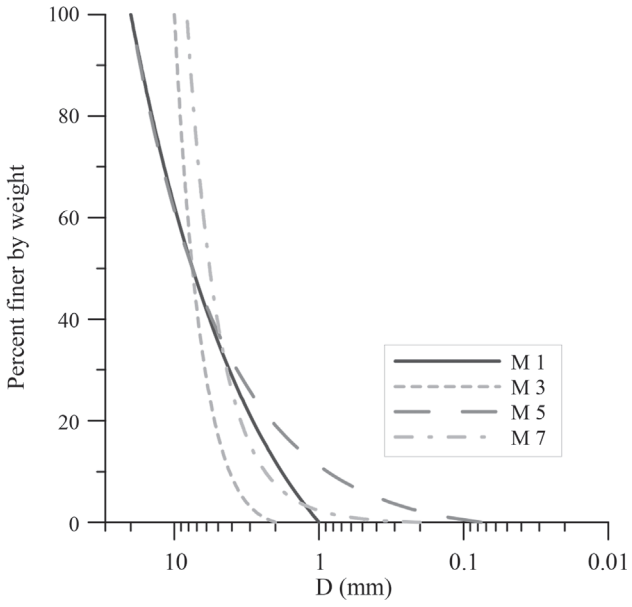

Figure 41 - Tested grain size distributions (Ramon *et al.*, 2008).

6. Rockfill Behavior Through DEM

Why does the Distinct Element Method (DEM) offer an interesting alternative to investigate the behaviour of coarse granular aggregates?

At least, for three reasons:

- Improving understanding of basic deformation mechanisms.
- It is a good complement to laboratory testing. Unlike fine soils, the number of particles in a laboratory test on gravels is within the practical limits of today's DEM capabilities.
- Even large structures, such as rockfill embankments, may be approximated through DEM in a not so distant future.

The performance of DEM to reproduce rockfill behavior has been investigated in recent years. Some highlights are given here.

The guiding idea was to develop a realistic model which could simulate three distinct aspects already discussed: scale effects, delayed (creep) deformations and environmental effects. The first aspect is particularly interest-

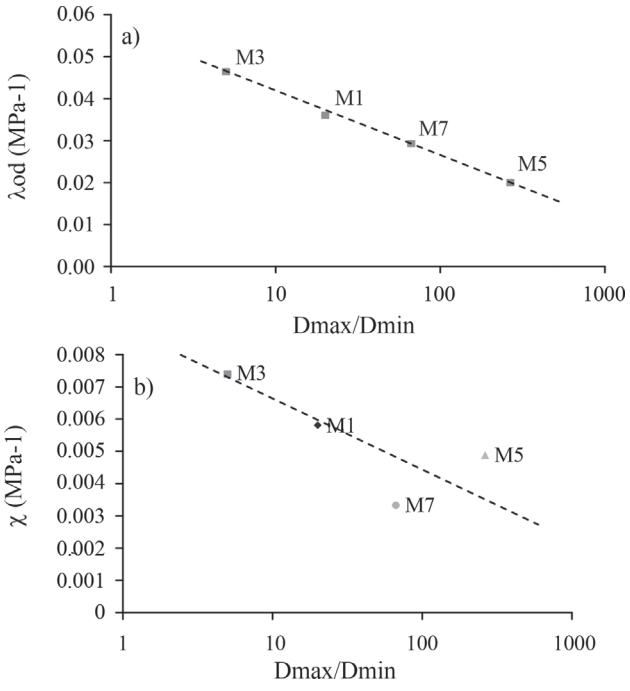

Figure 42 - Scale effects on: a) Compressibility parameter λ_0^d for unsaturated oedometer tests. b) Parameter χ . Grain size distributions are defined by the index D_{max}/D_{min} (Ramon *et al.*, 2008).

ing in practice because of the difficulty and cost of testing large samples in the laboratory. The model developed includes the following characteristics:

- Actual particle shape is reproduced in an acceptable manner.
- Particle breakage is introduced following some results from fracture mechanics. In particular, the subcritical crack propagation inside particles is the basic mechanism leading to the division of grains. In this way, time, scale (size) and humidity effects are automatically accounted for.
- A breakage protocol which tries to reproduce some experimental observations.
- Validation against actual testing results.

Figure 43 shows the DEM model of triaxial and oedometer samples of uniform gravel. The dimensions correspond to the equipment of the Geotechnical Laboratory of UPC.

Particle shapes are reproduced by aggregation of spheres. The starting geometry in all cases is a pyramid of 14 "microparticles" as shown in Fig. 44. The figure shows a gravel of a crushed limestone actually tested.

The selection of shapes implies a trade-off between geometrical accuracy and computational time. The basic code used in the simulations presented here is the PFC3D code developed by Itasca. An extensive programming of the basic kernel was required to include the simulation features outlined here.

The calculation relies on three basic steps:

1. Stress calculations on macroparticle.
2. Failure criteria for macroparticles.
3. Division of macroparticles and re-arrangement of the granular structure.

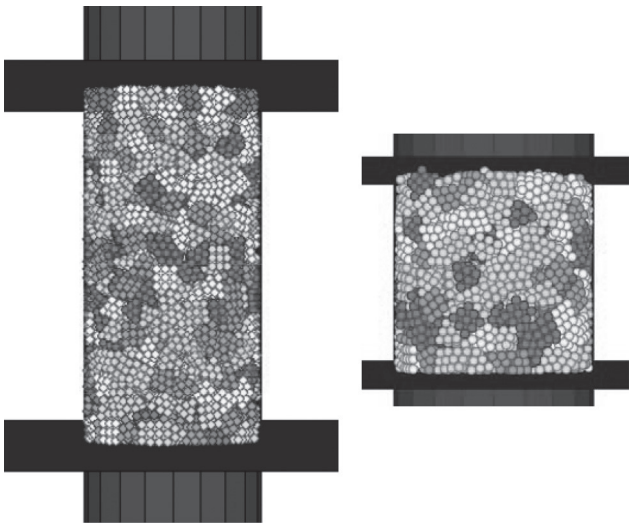

Figure 43 - DEM approximations of triaxial (height 0.50 m; diameter 0.25 m) and oedometer (height 0.25 m; diameter 0.25 m) samples.

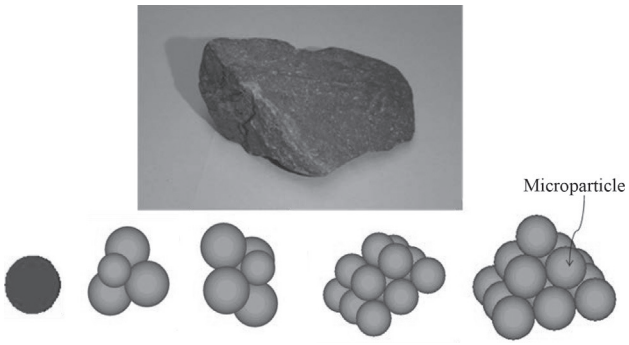

Figure 44 - "Clump" models of 1, 4, 5 and 14 microparticles.

The first step starts by identifying the maximum forces acting on each macroparticle of the sample. These forces are typically part of the force chains developed in the aggregate of particles. The calculation of tensile stresses inside each particle follows the closed form solution presented by Russell & Wood (2009) for loaded spheres. By introducing a set of flaws of randomly distributed flaw lengths in particles, a stress intensity factor, K, may be computed for each macroparticle.

The second step is summarized in Fig. 45 K is first compared with the rock toughness, K_c. If $K \geq K_c$ a particle division is applied in the manner explained below. If not, crack propagation starts following the velocity derived in Eqs. 4 to 7. When the size of the flaw, a, reaches half the equivalent diameter of the particle, a division is applied.

The third step is illustrated in Fig. 46. Two main possibilities are envisaged: either a "big" failure (crushing in equal volumes) or a contact crushing (comminution). The protocol is self explanatory in the figure. Note that once an isolated sphere is produced as a result of successive breakage, an additional fine division in small spheres is applied with the purpose of capturing better the generation of fines in the sample. The results given here correspond to a simple protocol of breaking (crushing in equal volumes) and fine subdivision is not applied.

The behavior of a uniform (D = 25-30 mm) hard limestone gravel subjected to oedometer and triaxial loading has been simulated. The main parameters are the friction coefficient at contacts, μ, the toughness, K_c, and the normal contact stiffness, K_n (shear stiffness was taken equal to normal stiffness in the simulations presented here). Consider first an oedometer test in which load was applied in steps, following the protocol, shown in Fig. 47. It corresponds to an actual test performed in the laboratory. Test results were used to determine parameters of the numerical model. Delayed deformations were measured at each loading stage and the sample was flooded at maximum vertical stress.

Model parameters were identified by fitting the compression curve and the evolution of the grain size distribution. This is shown in Figs. 48 and 49.

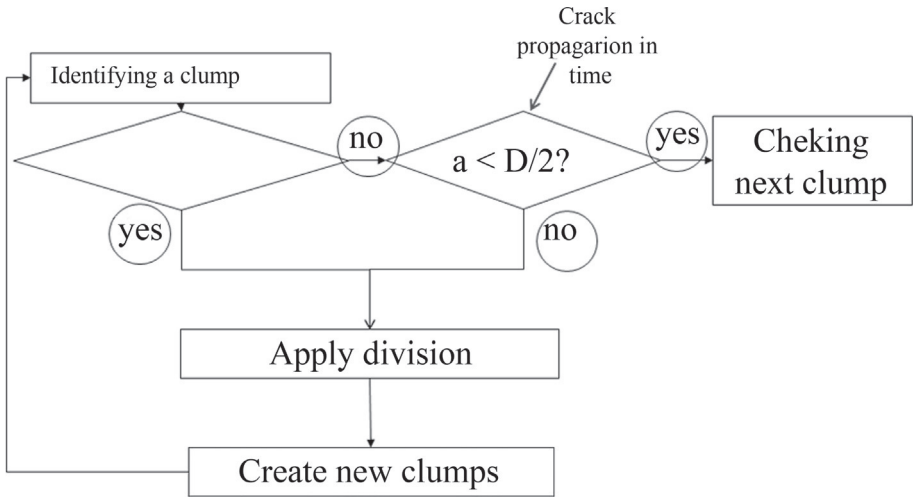

Figure 45 - Failure criteria for macroparticles.

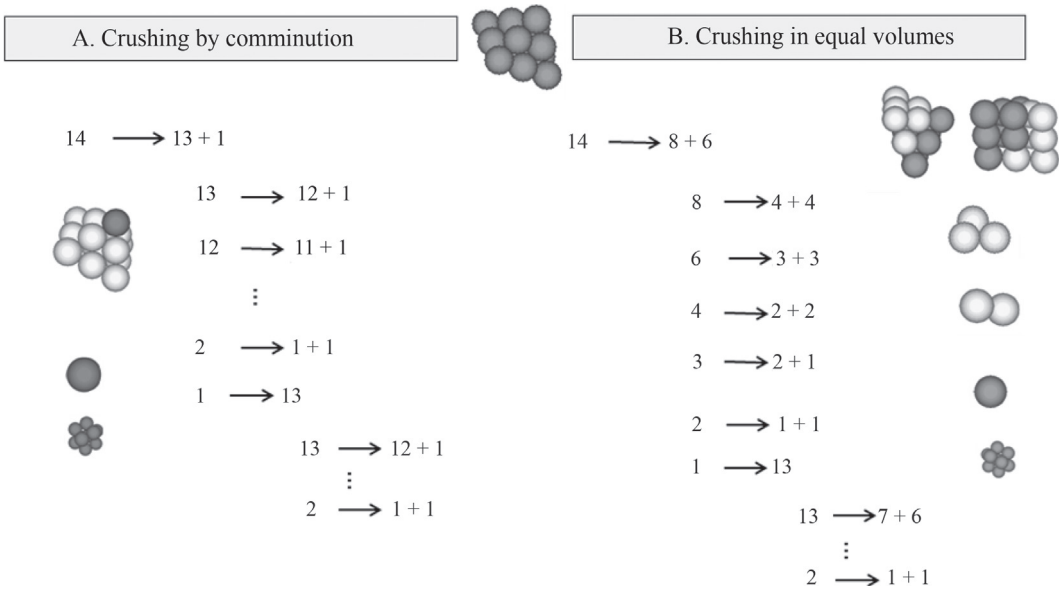

Figure 46 - Breakage criteria for a particle made of 14 spheres.

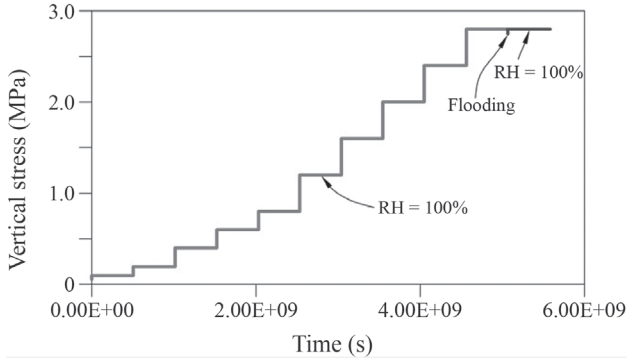

Figure 47 - Loading protocol of oedometer test.

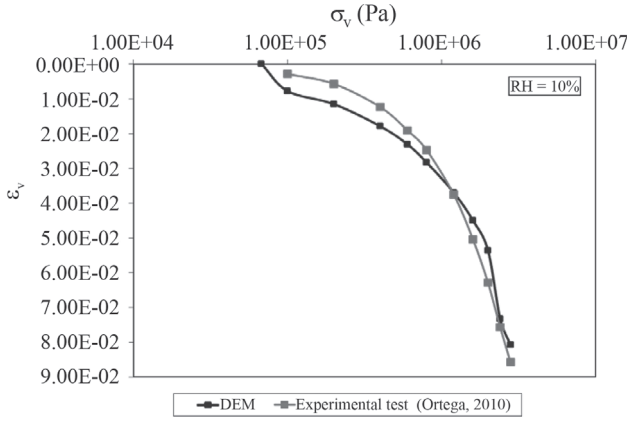

Figure 48 - Oedometer test on hard limestone gravel. Compression curve. Comparison of test results and DEM modeling.

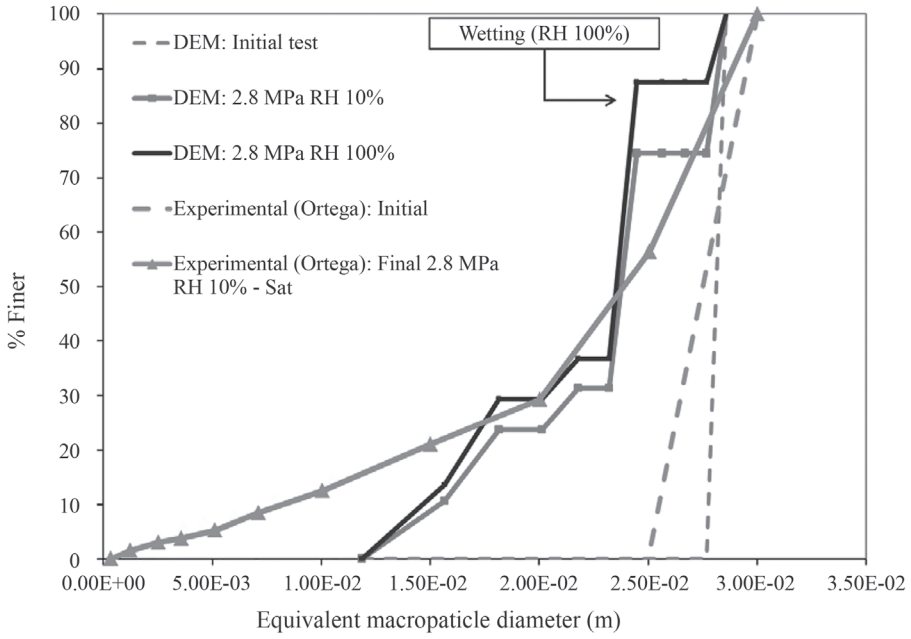

Figure 49 - Oedometer test on hard limestone gravel. Grain size distributions. Comparison of test results and DEM modeling.

The compression curve is well captured by the model. The evolution of grain size is not so well reproduced. The development of fines is limited by the minimum size of the microparticle selected. However, results are reasonable and the fitting allowed identifying the following model parameters: $\mu = 0.3$; K_c = 5e6 Pa.m$^{0.5}$ and the normal contact stiffness, K_n = 4e6 N/m.

Calculated delayed deformations for each loading stage are remarkably similar to actual test results. This is shown in Fig. 50. This result adds confidence to the set of assumptions made to build the numerical model. In particular, the subcritical crack propagation theory seems to offer a realistic framework to reproduce creep deformations of rockfill.

From a macroscopic perspective the oedometer test is just a particular stress path. It introduces some overall shearing, but it does not approach limiting shearing conditions. However, it may be argued that from a microscopic point of view it probably includes all the complexities of grain interactions, including grain breakage. It may be then accepted that the DEM model identified through an oedometer test is, in fact, a general model and, therefore, it should be capable of predicting the sample response under any other stress path. For instance, a triaxial test. This idea was checked by comparing the results of an actual triaxial

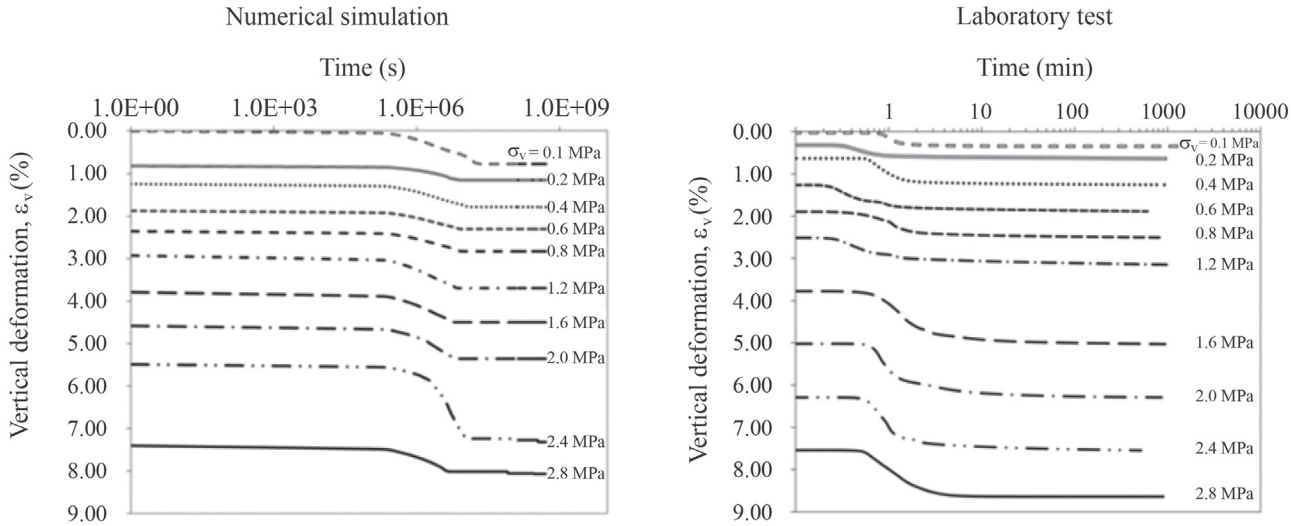

Figure 50 - Oedometer test on hard limestone gravel. Comparison of calculated and simulated delayed deformations.

test on the same crushed imestone gravel with the DEM prediction. The comparison is given in Fig. 51. The laboratory test was run under "dry" conditions and it was flooded when strength conditions were reached. This is why experimental results are limited to a maximum deformation of 10%. The stress-strain curve is very well reproduced by the model. This is an encouraging result.

However, measured volumetric deformations are higher than DEM predictions. This is probably a consequence of the particle division protocol used in this simulation, unable to enter into the fine particle divisions.

The capability of the model developed to explore size effects will now be illustrated. The objective is to know the effect of grain size on the oedometric compressibility. The formulation of the analysis is summarized in Fig. 52.

Particle sizes of initially uniform samples were selected in a wide range (2.8 mm to 0.56 m). Four samples were built, having all of them the same initial porosity (n = 0.53). The sample size, also given in Fig. 52 illustrates the difficulties of laboratory testing. A sample of boulders having a mean diameter of 56 cm would require a diameter of no less than 5 m to maintain a reasonable diameter to particle size ratio. Even for gravels of no more than 14 cm in size the oedometer diameter reaches 1.25 m in order to preserve the same diameter/particle size ratio. The numerical tests were performed under "dry" conditions at a RH = 10%.

The calculated compressibility curves are given in Fig. 53. The compressibility coefficient was calculated in the final part of the curves, for stresses in excess of 1 MPa. They are represented in Fig. 54.

Also indicated in the figure are three experimental values determined by Ortega (2008) in experimental tests. They occupy a relatively narrow range but they help to add confidence to the simulation.

Obviously DEM could be applied to investigate the effect of particle size on any constitutive parameter. In a more general case, particle "size" could be changed into

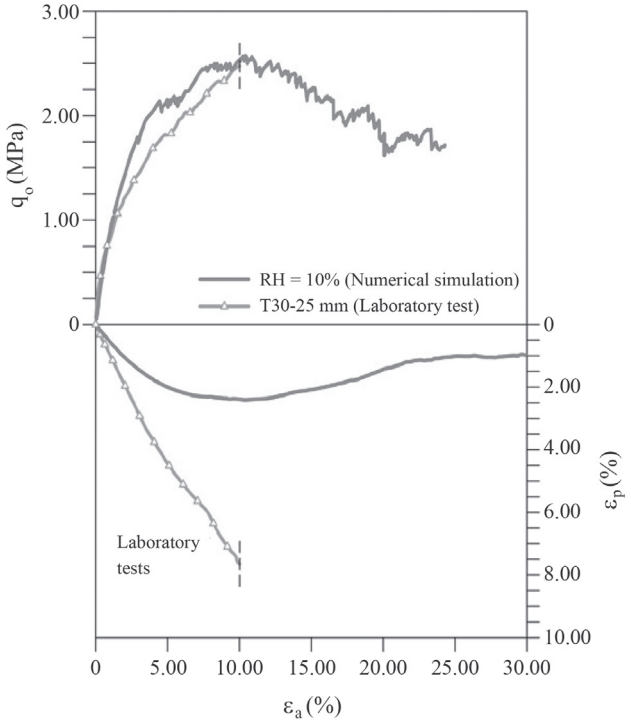

Figure 51 - Triaxial test on hard limestone gravel. Comparison of calculated and simulated DEM results.

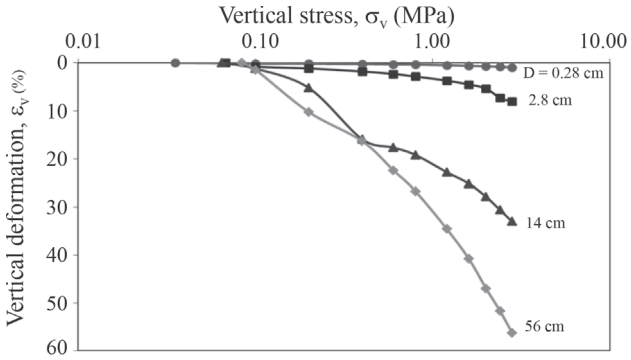

Figure 53 - Simulated oedometer tests on samples of different initial uniform grain sizes.

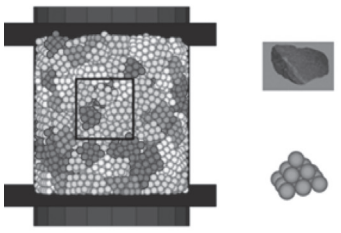

Contact stiffness, kN: N/m	4 x 10^6
Shear stiffness, ks: N/m	4 x 10^6
Friction coeficiente, μ	0.3
Toughness, K_c: Pa.$m^{1/2}$	5 x 10^6

Sample	Relative scale	Sample size: Height (mm)	Sample size: Diameter (mm)	Equivalent macroparticle diameter (mm)	Initial porosity
S25	0.1	25	25	2.8	0.5314
S250	1	250	250	28	0.5314
S1250	5	1250	1250	140	0.5337
S5000	20	5000	5000	560	0.5314

Figure 52 - Size effects on confined compressibility. Data for DEM analysis.

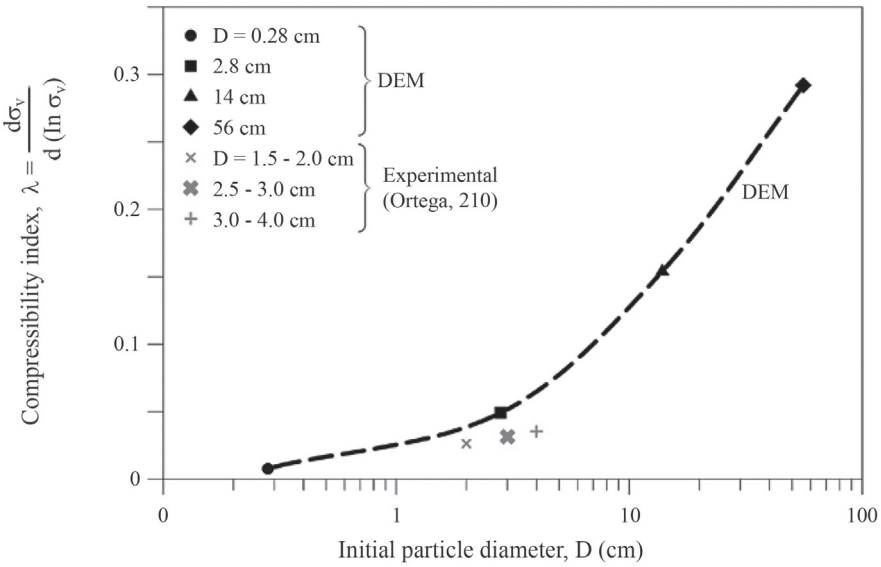

Figure 54 - Variation of oedometric compressibility index with initial grain size.

grain size distribution, a possibility which is beyond the possibilities of some theoretical approximations (Frossard *et al.*, 2012) based on a given initial size distribution.

7. Behavior of Rockfill Embankment Under Rainfall Action

An interesting case that shows the capability of the elasto-plastic rockfill models is the response of a rockfill embankment 40 m high (Fig. 55) located in the Madrid-Seville high-speed railway. The rockfill was made of compacted schists. Figure 55 shows a good correlation between the rainfall intensity and the velocity of the crest settlements. The correlation is excellent for three periods of intense rainfall in 1994, 1996 and 1997. However, the final period of intense rainfall represented in Fig. 55 did not result in any significant acceleration of the motions.

This case will be analyzed with the purpose of investigating the effect of some key parameters. Fig. 55 also indicates that there is a constant base velocity not affected by rain, which can be identified as a pure creep phenomenon. It is clear that the rockfill deformation models should include creep if they are to be used to simulate long-term behavior. The experimental tests mentioned before indicate that this basic creep is also controlled by RH.

In order to study this case, the finite element program Code_Bright (Olivella *et al.*, 1994, 1996) was used. A rockfill embankment, 40 m in height with symmetric slopes (1V:3H) and a crest width of 8 m, was modelled. The elastoplastic formulation of the model used has been described in Oldecop & Alonso (2001) and Alonso *et al.* (2005).

Table 1 collects the set of constitutive parameter describing the rockfill. The properties of the rockfill embankment of the Seville-Madrid line are not known in detail

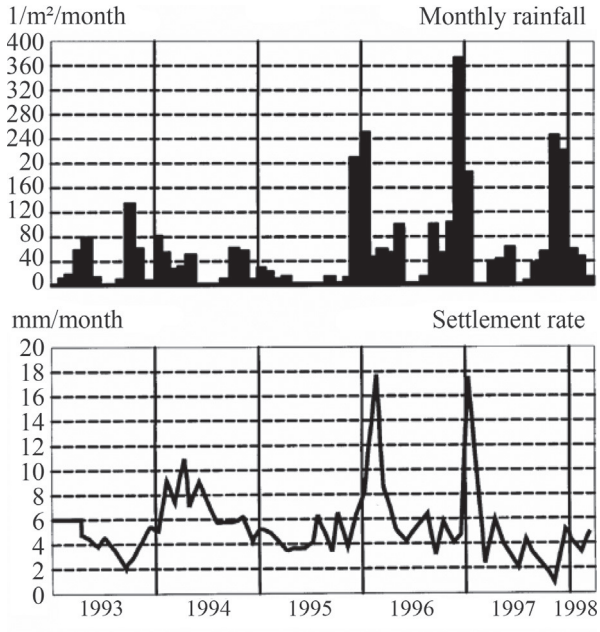

Figure 55 - Rockfill embankment in Madrid-Sevilla high speed railway line. Correlation between settlement rates and rainfall (Soriano & Sánchez, 1999).

(Soriano & Sánchez, 1999 only offer a brief description). However, the set of available data for Beliche dam for a material which is similar to the material used for the railway embankment are a good starting point to develop the calculations in this case.

The analysis performed focused only in three parameters: the air entry value of the retention curve of the compacted schist, p_0, the creep parameters, μ, and the intrinsic permeability. The solved cases are grouped in Table 2. The initial state of the embankment is characterized by an initial

Table 1 - Mechanical and hydraulic constitutive parameters for the simulation of the rockfill embankment.

I. Elastic behaviour			
Elastic modulus	E	MPa	150
Poisson coefficient	ν	-	0.3
II. Plastic behaviour			
Plastic instantaneous compressibility, virgin	$\lambda^i - \kappa$	-	0.025
Clastic virgin compressibility for saturated conditions	λ_0^d	-	0.028
Parameter describing the variation of clastic compressibility with total suctionl	α_s	-	0.010
Slope of the strength envelope at critical state. Dry conditions	M^{dry}	-	1.75
Slope of the strength envelope at critical state. Saturated conditions	M^{sat}	-	1.30
Parameter controlling the increase of cohesion with suction	k_s	-	0
Mean threshold stress for the development of clastic deformations	p_y	MPa	0.01
Parameter to define the associativity of plastic potential	α	-	0.3
III. Hydraulic properties			
Intrinsic permeability	k	m/s	Back analyzed
Van Genuchten parameter describing the air entry value	p_0	MPa	Back analyzed
Van Genuchten parameter describing the slope of the water retention curve in its intermediate range	λ	-	0.33

average yielding stress, $p_o^* = 0.04$ MPa. An initial constant suction $s_0 = 1.5$ MPa was imposed to the whole structure.

An equilibrium stage was first calculated (in this phase the boundaries are assumed to be impervious). The initial void ratio is $e_0 = 0.5$. The calculated response of the embankment as a result of the rainfall record is given in Fig. 56. Settlement rate and the evolution of suction in a particular representative point at the base of the embankment are given. The correspondence between calculations and "in situ" measurements is very poor. In fact, the model indicates that most of the collapse occurs during the first year and a half, when, the rockfill was exposed to a moderate rainfall. Beyond this initial settlement phase, the calculated suction remained essentially constant and the model did not predict any further settlements.

Consider now, Case B. The only change introduced is an increase in air entry value ($p_0 = 0.1$ MPa). In this way the material may store more water at any applied suction. Figure 57 shows the result of calculations. They now show a much better agreement between model and measurements. Rainfall records of 1993 and 1994 produced a moderate collapse. The strong rainfall, at the beginning of 1996 and 1997 triggered a fast acceleration of settlements, which is also predicted by the model. At the beginning of 1997, before the rainfalls of 1996, the suction in the embankment reaches its lowest value and the collapse potential disappears. This explains the lack of reaction when facing the upcoming strong rainfalls at the end of 1997. At that time, the embankment maintains the water in an efficient way and suction is kept below the values calculated for Case A.

Table 2 - Rockfill embankment. Madrid-Sevilla railway. Analyzed cases.

Case	Air entry value, p_o (MPa)	Flow parameter, μ (MPa^{-1})	Intrinsic permeability (m^2)
A	0.01	0.0012	10^{-9}
B	0.10	0.0012	10^{-9}

The settlement velocities calculated and presented in Fig. 57 underestimated the field measurements in moderate or non-existent rainfall periods. Suction is clearly maintained constant during these periods of time and the reason for a constant rate of settlement is a creep phenomenon. Increasing this component improves the reproduction of the field records.

Figure 58 offers an additional analysis of the collapse mechanisms associated with rainfall and the specific water retention properties of the rockfill. The figure illustrates the stress paths (p, s) in a reference point, of the rockfill embankment for Cases A and B. The points highlighted in the plot refer to specific times, which are also shown in the figure. Also indicated is the position of the LC yield curve at some specific times. The intensity of the collapse is directly related to the displacements of the yielding point along of axis p. The stress path for Case B displaces towards the right because the vertical net stress increases with the increasing water content of the rockfill, which is controlled by the retention curve. The large displacements of the yield curve in Case A during the first wetting episode (rainfalls in 1993-1994) induced large collapse deformations. The low suction that is reached later on indicates the slight possibil-

ity that some additional collapse may occur. On the other hand, the rockfill described by Curve B loses suction more gradually and the displacements of the yield curve are smaller. At the end of the first rainfall period, the existing

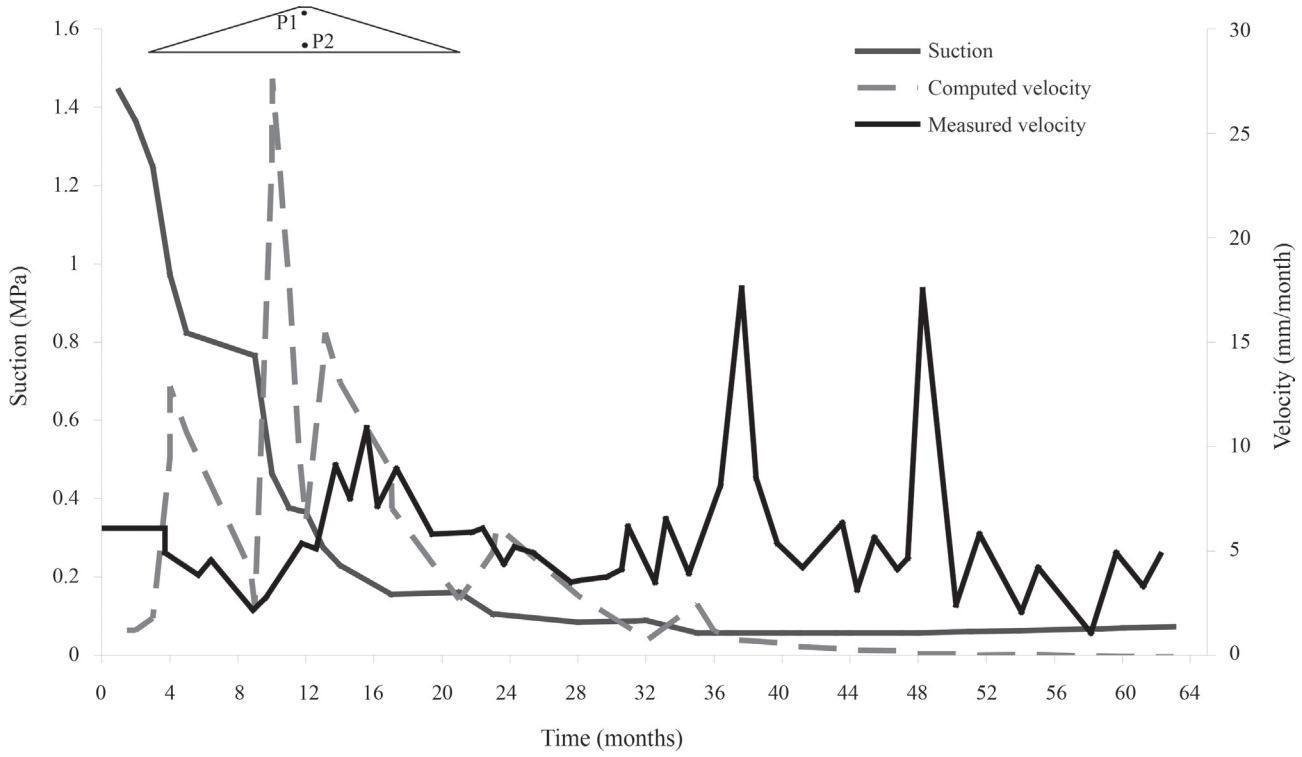

Figure 56 - Case A. Comparison of measured and calculated settlement rates in point P1. Also shown are suction changes in point P2 (Pinyol *et al.*, 2008).

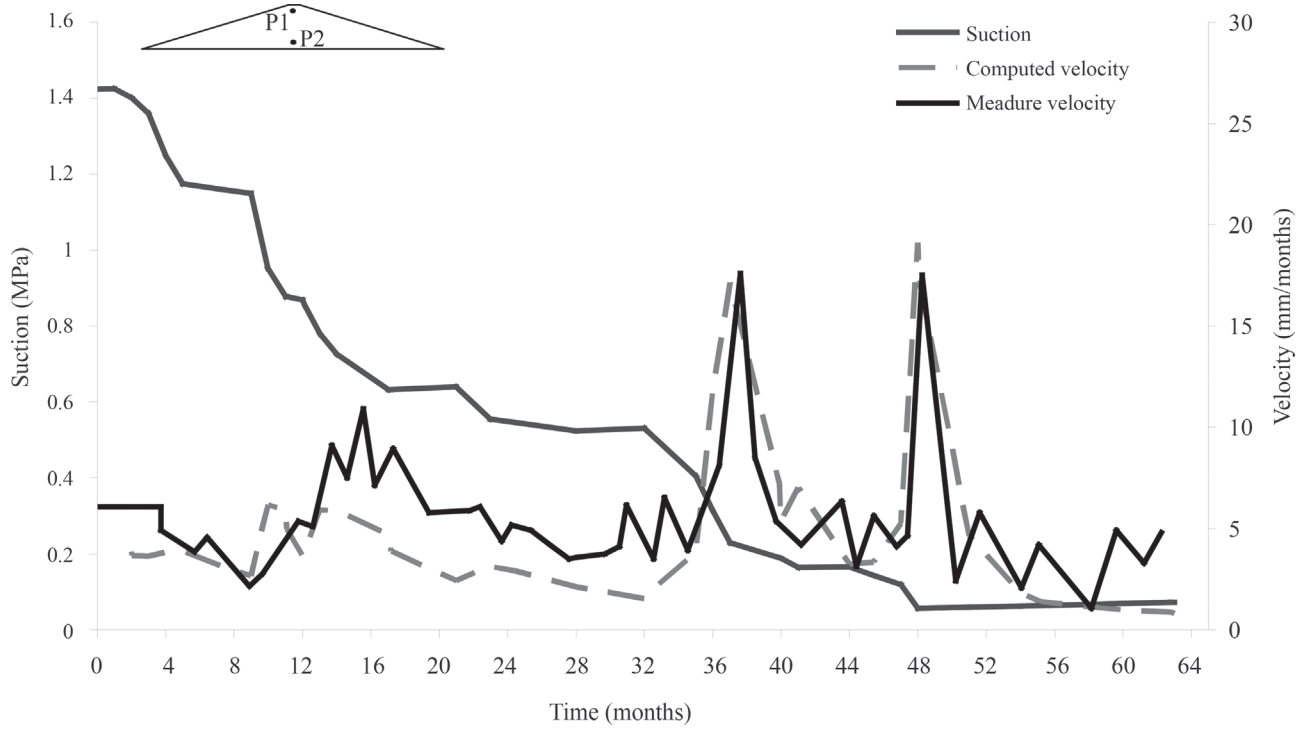

Figure 57 - Case E. Comparison of measured and calculated settlement rates in point P1. Also shown are suction changes in point P2 (Pinyol *et al.*, 2008).

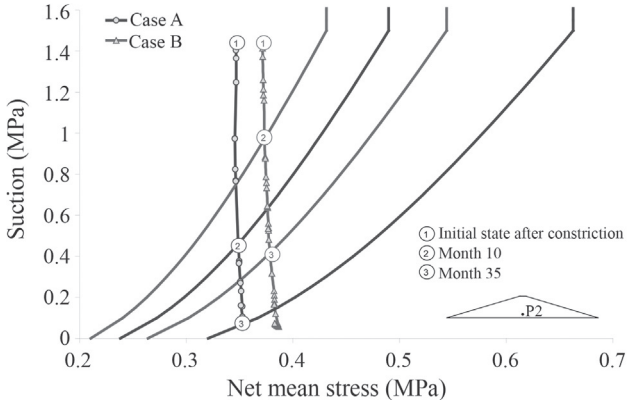

Figure 58 - Stress-suction paths for point P2 in cases A and B. Also show is the evolution of isotropic yield locus (Pinyol *et al.*, 2008).

suction still has significant collapse potential. Note that due to the shape of the yield curve, the changes in suction in the low range of values are especially effective to induce significant collapse.

This case demonstrates that the water retention curve of the materials has a large effect in the development of collapse settlements in time for a given rainfall regime. However, the intrinsic permeability has an insignificant effect. The time necessary to produce settlements, due to humidity changes, is controlled not only by some key properties of the rockfill (those which characterize the retention properties of water), but also by the specific rainfall regime. Extreme rainfalls induce more collapse settlements only if they imply an additional increase in RH beyond the maximum value reached previously. Creep deformations also depend on the weather, because RH controls delayed deformation, as explained above. Creep deformations also affect hydraulic collapse, because they are irreversible volumetric deformations that harden the material. A hardened fill reacts with lower collapse potentials against any new wetting episode. In practice, distinguishing between long-term deformations induced by wetting or by pure creep is not easy. However, deformations induced by changes in water content tend to concentrate in singular rainfall events that take place in a relatively short time.

8. Beliche Dam

Beliche dam is a remarkable case in the literature of rockfill dams because of the wide interest given to this case by many research and technical groups. In addition to several papers published in Géotechnique (Naylor *et al.*, 1986, 1997; Alonso *et al.*, 2005) the dam has received a considerable attention in Doctoral dissertations and other Conference and journal papers. There are some reasons for this interest: the dam behavior was well documented, the LNEC performed a singular set of large diameter tests on the material of dam shoulders and the behavior of the downstream shell was rather unexpected. In fact, measured settlements were as high as those measured upstream when the reservoir was filled. The case has been analyzed from the perspective offered by the conceptual and mathematical models described in this paper (Alonso *et al.*, 2005)

The mechanical parameters of the elastoplastic model developed (Rockfill model; Alonso *et al.*, 2005) were determined by back-analyzing tests reported in Naylor *et al.* (1986, 1997). Figure 59 provides a comparison of measured results and model performance for an oedometer and a triaxial test. Flooding the triaxial test at an advanced state of shearing provided interesting information, which could be well reproduced by the model. The agreement shown in Fig. 59 is reasonably good with the exception of the dilatant behavior of the triaxial sample. This is a shortcoming of the model, which was described, in the (q, p) plane by regular ellipses.

The rockfill model is one in the library of models available in Code-Bright and has been used in the analysis of several earth and rockfill dams after the pioneering work conducted in Beliche.

Figure 60 shows the pore pressure evolution of four points (1, 2, 3, 4) located in the lower part of the dam. Two of them are located in the upstream inner shell (1) and in the core, close to the upstream boundary. Points 3 and 4 are their downstream symmetric counterparts. The upstream locations essentially follow the reservoir elevation and they exhibit positive pore pressure values at an early stage in the simulation. Situation "*E*" (at a time t = 1440 days) is not yet at steady state conditions. The map of pore pressures inside the dam is also given in Fig. 60 for the same time. The saturation line displaces slowly inside the core as an approximately vertical front.

Pore pressures of the downstream location are negative (suction) and they essentially reflect the rainfall history. In the simulation performed, due to the high permeability of the exposed shoulders, the total precipitation was imposed as an external flow rate. Evapo-transpiration from the rockfill shoulders is probably minor in this case. Most of the oscillations in suction plotted in Fig. 60 take place in an elastic regime (at essentially constant mean stress). However, whenever suction reaches a lower value than any other suction value in the past record, irreversible strains will develop, leading to dam settlements.

This is illustrated in Fig. 61, which shows a map of plastic volumetric strains at time "*E*" and the history of these irreversible strains during the early life of the dam. Note that calculated deformations of points 1 and 4, located in the inner rockfill shell, upstream and downstream of the impervious core essentially develop similar strains despite the fact that the upstream point was fully saturated at an early time and Point 4 never experienced saturated conditions if suction calculations are correct. In fact, a low suction is capable of maintaining these materials essentially "dry" because of their very low air entry value. The deformation map shows a fairly symmetric distribution of strains

with respect to dam axis. The flowing water through the core, however, enhances the volumetric deformations of the upstream part of the clay core.

Calculated and measured vertical strains at three different positions and at five different times are compared in Fig. 62. The comparison is good for the dam axis (core).

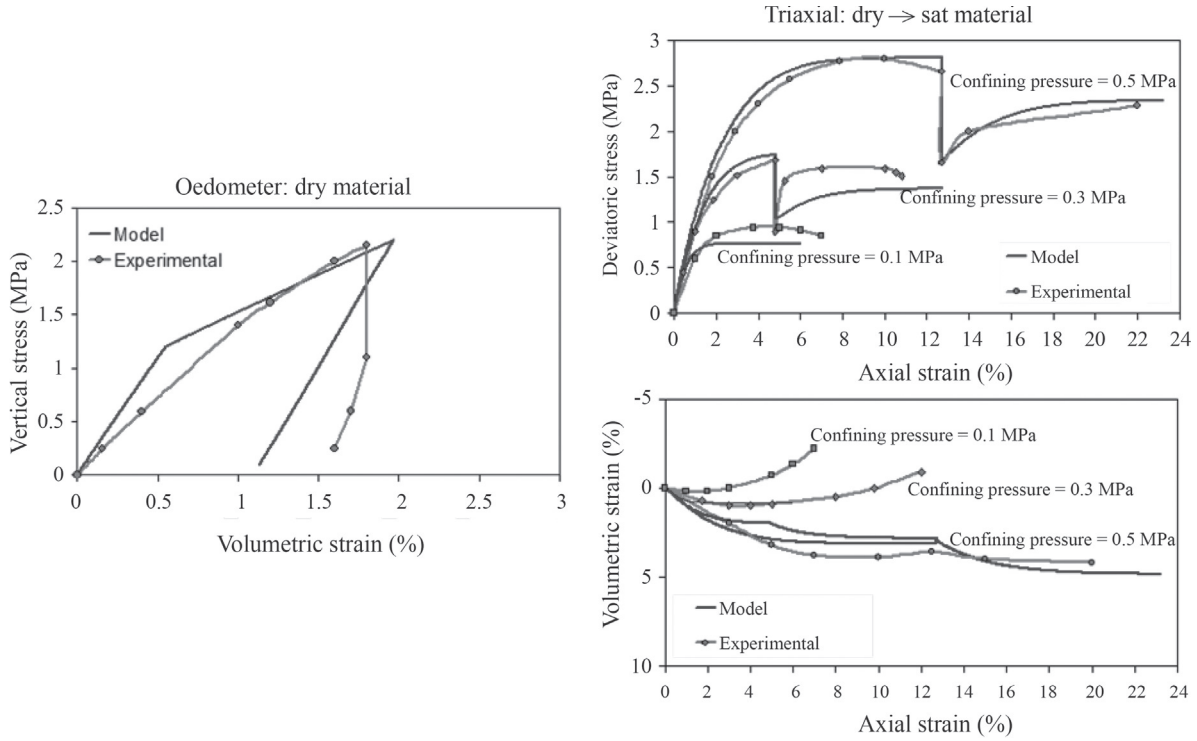

Figure 59 - Modelling oedometer and triaxial experiments of Beliche dam greywacke outer shell.

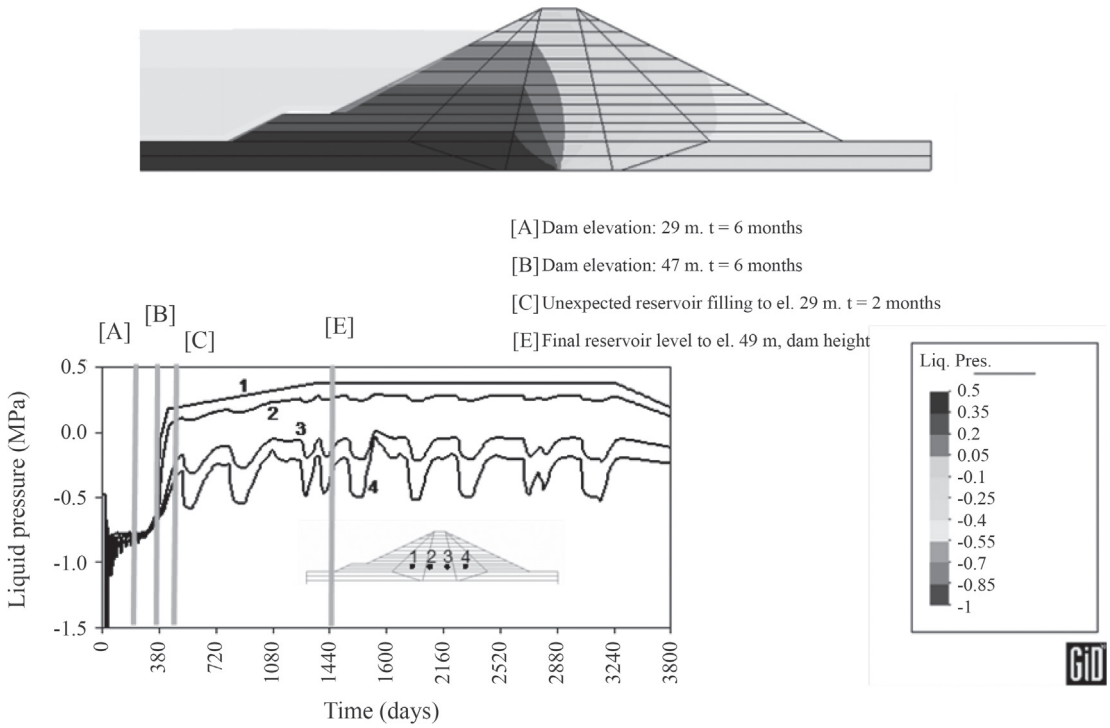

Figure 60 - Beliche dam. Pore water pressure distribution at time (*E*) and evolution of pore pressures at four points (1, 2, 3 and 4) located in the lower part of the dam.

Field deformations are higher than calculated ones in the rockfill shells. It should be noted that predictions were based on laboratory test results. Two modifications led to a better fit: the introduction of size effects in the manner discussed in this paper and the consideration of creep strains.

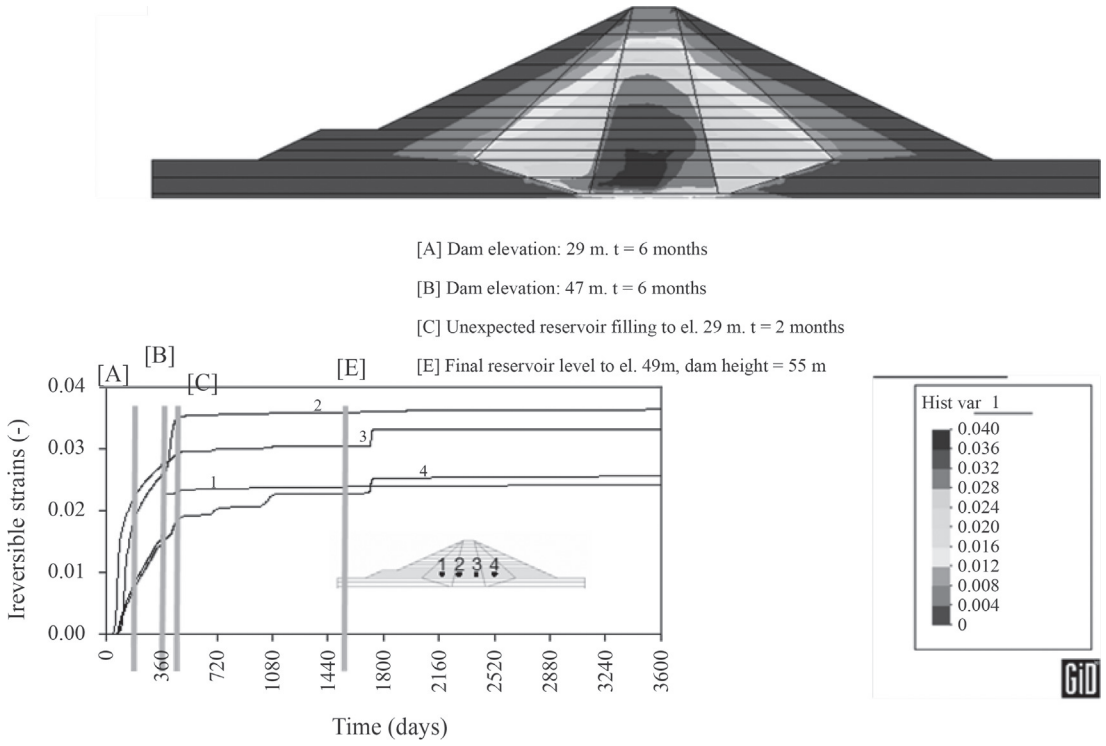

Figure 61 - Beliche dam. Map of plastic volumetric deformations at time (*E*) and evolution of plastic volumetric strains at four points (1, 2, 3 and 4) located in the lower part of the dam.

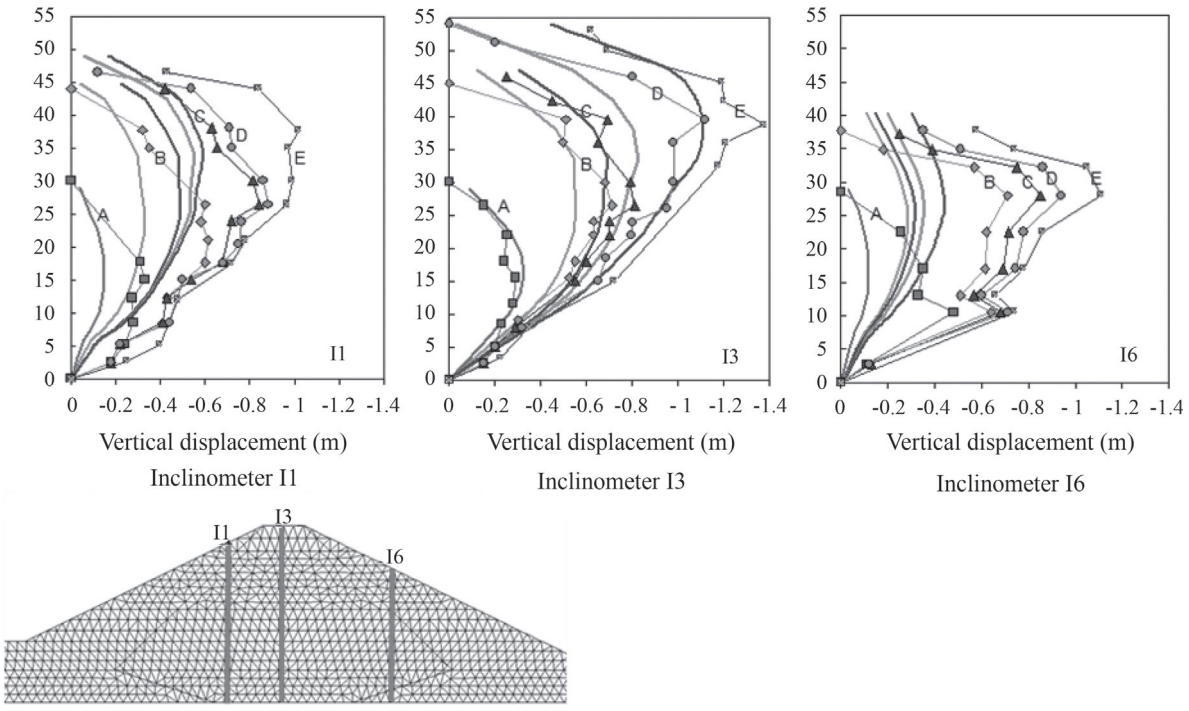

Figure 62 - Comparison of recorded and calculated vertical strains at five different times at the position of extensometers I1, I3 and I5.

Figure 63 shows the measured and calculated surface displacements of a marker located on the downstream shell. Vertical settlements are particularly well captured. Settlements increase suddenly at the time of intense rainfalls. The calculated records of (negative) pore pressures at the base of the inner downstream shell provide a nice explanation: Settlements are the result of collapse strains which are induced when suction reaches a value lower than any value in the previous history of the shell. For most of the time the rockfill remains under elastic conditions, except for the unavoidable sustained creep explained by a progressive breakage of particles subjected to a subcritical propagation of cracks.

9. Epilogue

The behavior of coarse granular materials, described in this paper, requires for its correct interpretation, a wider framework, the one offered by the mechanics of unsaturated soils. This epilogue recalls this wider framework with the purpose of providing a reference to the developments described here. It is interesting to start describing the recent evolution of knowledge of unsaturated soils.

After a large stage dominated by empiricism, during the 80's of the 20th Century, the systematic research on the mechanical behavior of unsaturated soils started. It could be thought at that time that a unique theory would perhaps be able to solve in a satisfactory and complete manner the effect of lack of saturation in soils. When some papers on

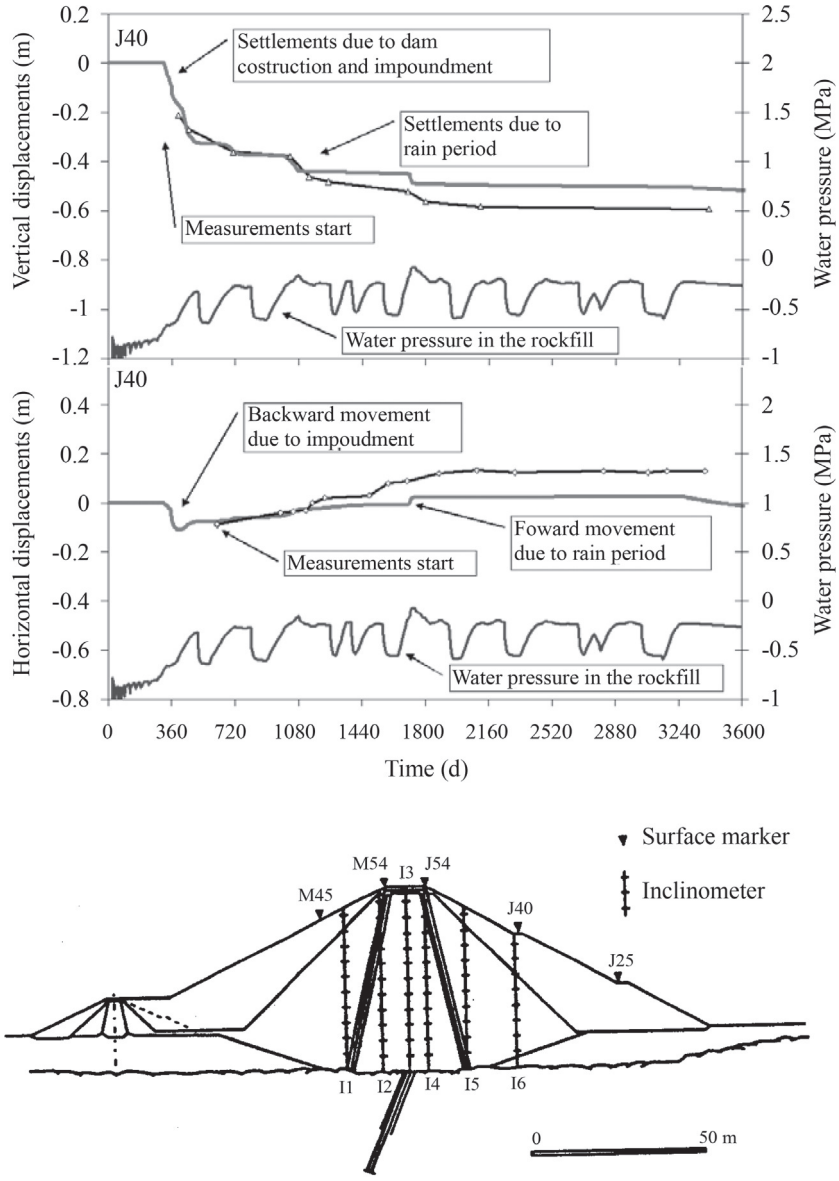

Figure 63 - Measured and calculated surface displacements of downstream marker J40. The evolution of calculated water pressure in the inner downstream shell (Point 4 in previous figures) is also indicated.

fundamental research are examined, the impression is that the authors look for this general paradigm.

However, the situation progressively unfolded was more complex and exhibited more difficulties than initially expected. In the 90's attention started to be paid to the microstructure of soils and more specifically to the size and distribution of pores. In fact, the intensity of the capillary forces is directly related to a radius of curvature of the air-water interfaces which could develop in pores. This focus on microstructure is still very active in the fundamental research of unsaturated soils.

Laboratory research concerns frequently a limited class of soils: silts and clays of low plasticity. The reasons for this situation are easy to understand: these are materials where the capillary concepts are of direct application and moreover their permeability is sufficiently high so as to allow relatively reduced testing times. These soils are often fabricated by static compaction, which reduces heterogeneity. Their void ratios are high, which ensures a response easily measurable with the equipment available in the laboratory.

This trend, which is justifiable in university research, neglected a great amount of natural soils and construction materials (compacted soils from any conceivable geological formation), and in particular, rockfills and gravels. In fact, most of the interesting soils in practice were left outside fundamental research.

Fortunately, the need to solve some new problems, of great significance due to their relationship to safety issues (a singular example would be radioactive waste storage in deep geological repositories) forced the attention towards materials that do not share some of the favorable circumstances mentioned before. There was a need to investigate very expansive and very dense materials (compacted bentonite, either pure or mixed with sand or well-compacted in high-density pellets). Those are very impervious materials, in which the physical and chemical aspects (as opposed to capillary aspects) are significant in order to examine their relationship with interstitial water.

At the other extreme of grain size distribution, many orders of magnitude above, another class of materials, gravels and rockfill, was known for a long time to be sensitive to the presence of water. It was also known that they deform as a consequence of the breakage of particles, but the relationship between particle breakage and the presence of humidity was not well understood. The behavior of these materials brought again the concept of suction.

The fundamental deformation mechanisms of the wide range of natural, as well as compacted soils, lead to the abandonment of the idea that the unique constitutive framework could be applied to all granular materials just because they were unsaturated. Specific attention should be paid to the physics of deformation at an elementary level, at particle or pore scale.

Let us review the effect of suction in different soils, characterized, as a simple criterion, by grain size. This discussion has been synthesized in Fig. 64.

- The size of particles in rockfills and gravels varies approximately between diameters separated by two orders of magnitude: centimeters and meters. Deformation, as

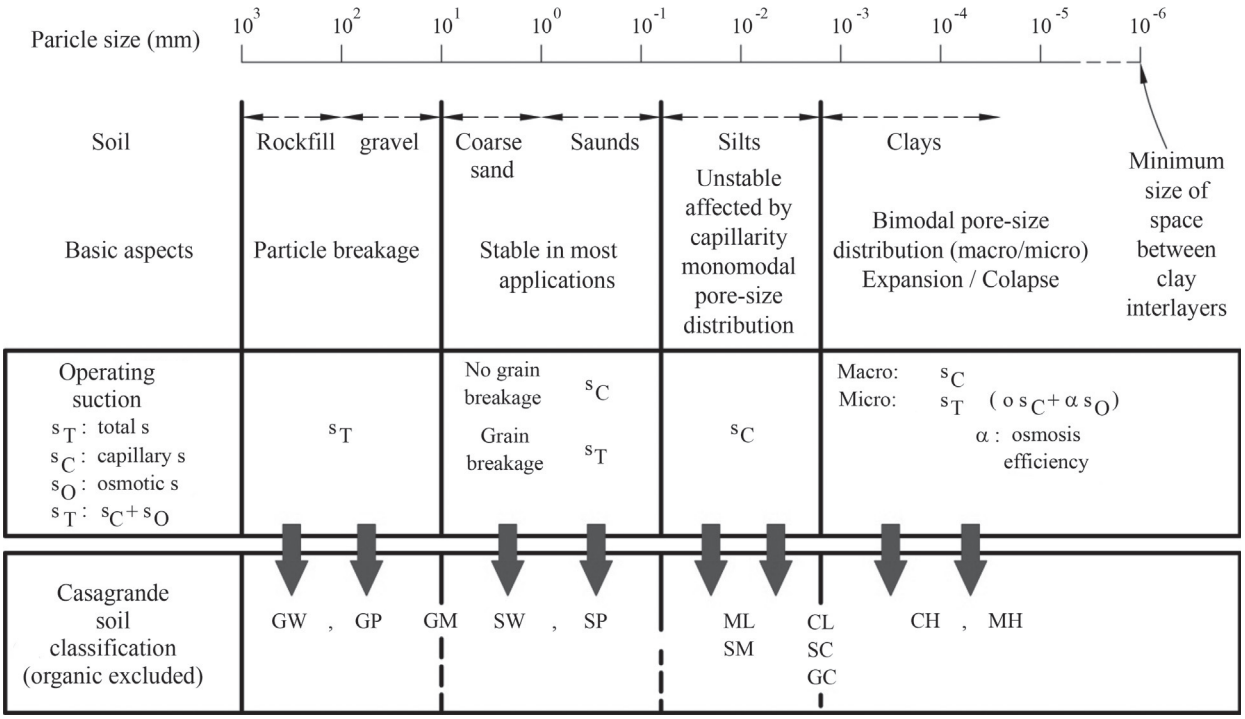

Figure 64 - Type of soils and operative suction.

explained in this paper, is dominated by the breakage of particles (fragments of rock) and the subsequent rearrangement of the granular structure. The breakage of particles is associated with the propagation of fissures in rock fragments.

- Fracture is possible because the size of the grains results in a low number of contacts per unit area or unit volume of the aggregate. On the other hand, the weight of the aggregate only depends on the density and global porosity, and those are magnitudes that essentially do not change with grain size. As a result, concentrated loadings inside the rockfill increase with the size of the grain. Their intensity is high enough to reach stress intensity factors which are close or above the toughness of rocks. This facilitates the propagation of fissures. RH controls also the velocity of the propagation of fractures. The velocity increases when the water energy is high (high RH). One alternative measure of this energy is total suction, directly related to the RH.
- When the grain size decreases to 10^{1}-10^{-1} mm, we are in the presence of sands. The number of contacts per unit area (for a given reference stress which remains unchanged) increases substantially if compared to gravel and rockfill. Conceptually, this is an "scaled" material of rockfill and gravel, but in this case the concentrated loading at the contacts decrease substantially. The stress intensity factor, which can be calculated in loaded particles, is small, and it is far from the toughness of the rock or mineral that constitutes the grain. Therefore, unless external stresses are very high, those derived from explosions, for instance, the breakage of particles is irrelevant. Therefore the effect of RH in the deformation of these materials disappears. However, if the particles (and therefore the pores) decrease in size (which is the case in fine sands), capillary forces begin to increase. These forces become closer in intensity to the forces between particles originated by the soil weight or the loads of foundations and structures. Therefore the variation of these capillary forces has a particular effect on the mechanical behavior of fine sand. This effect remains small. In any case, it is controlled by the capillary suction.
- In silts, which are materials without plasticity and whose particle sizes range between $8x10^{-2}$ and $2x10^{-3}$ mm, the capillary forces become much more intense. They are now similar or higher than those originated by soil weight or by the external loads. Again capillary suction is the "effective" component of the total suction. Capillary suction increases the resistance and stiffness of these materials. Microstructure continues to be simple. The pores are typically distributed around a single dominant pore size.
- The transition towards clay soils implies a fundamental change. On the one side, there is often a bi-modal structure of pores, characterized by two main sizes, separated by several orders of magnitude. They are the "macro" and "micro" components of the soil structure. On the other side, the capillary concept, which is still interesting to understand the macro behavior, loses its utility in the micro behavior, in which physical and chemical phenomena that link water to mineral surfaces predominate. The small size of the spaces between clay crystals or laminae suggests that the clay aggregates may act as semi-permeable membranes, at least to some extent. This idea and some experimental results suggest that the suction that controls the deformation of aggregates is total suction, although the osmotic component would be probably affected by a reduction factor. In this way, a more complete framework to understand the effect of suction on the behavior of clays may be developed. Capillary suction controls (as in granular media) the arrangement of aggregates. The total suction will explain the deformation of the aggregates themselves.
- Other materials. The idea of resorting to the size of particles to describe the type of soil is useful to explain the fundamental concepts, but it is far from giving a precise description of actual soils. The soil classifications, in particular Casagrande classification, are a resourceful alternative. In Fig. 64 there is a proposal to relate the type of soil (GW, GP. CH, MH) to the "operative" suction to explain the mechanical behavior. Some soils are easy to assign because they directly reflect grain size distribution. Others occupy transition spaces. Among them a very wide class of natural and compacted soils may be found. They are the medium to low plasticity clays, and mixtures of silt-clay, or even gravel-clay.
- Those materials often exhibit a double structure, but physical and chemical phenomena of clay-water interaction are less remarkable than in high plasticity clays. Their expansivity is also lower and this implies that "simpler" constitutive models, such as BBM (Barcelona Basic Model; Alonso *et al.*, 1990), can be applied. Figure 64 does not include all the soils of interest in geotechnical engineering. In fact, cemented soils are a wide class of materials, which are often unsaturated in practice. This is the case of loess, alluvial soils in arid and semi-arid climates, residual soils and tropical soils.
- Finally, soft argillaceous rocks are frequent in geotechnical projects. They are typically materials somewhat cemented and having low porosity. Their degradation against atmospheric cyclic action can be analyzed with some advantage from the perspective of the mechanics of unsaturated soils. They are soils that exhibit properties shared with gravels and rockfills (when the suction is high, that is, when they are dry) and clay and silts (when the suction is low).

The groups of soils identified previously required constitutive models which are differentiated, simply because the mechanism of deformations and the nature of suction controlling the behavior are different. Despite this, the models developed show some dependency among them,

which contributes to provide some additional order to the described scenario.

In the core of this order we may locate the models that are developed around the concept of yield function LC (Loading-Collapse), which has been described in this paper although its origin started with the BBM. The fundamental contribution of these models is to link the behavior under load to the collapse phenomenon, which is a key characteristic of the lack of saturation in a granular medium. The BBM reproduces in a reasonable manner the behavior of low to medium plasticity soils. It was formulated in terms of two independent stress fields: net stress and capillary suction. When examining, in one of the extremes of the grain-size distribution, the behavior of gravel and rockfill, there are interesting similarities with this basic model developed for conventional soils. In fact, the model described in Section 4, could be also called an "LC" type of model even if the collapse mechanisms are very different from those found in soils. Suction has no a stress or capillary interpretation. Rather, it is the energy interpretation of suction, associated with its role in fracture propagation, which explains the laboratory and field observations.

Acknowledgments

The author wishes to thank the excellent work performed by his past Doctorate students, Prof. L. Oldecop, Prof. C. Chávez and Dr. E. Ortega. Their findings and test results are at the core of this lecture. Thanks are extended to Dr. N. Pinyol and Prof. S. Olivella who helped the author in all computational aspects. The chapter on DEM modeling is part of the ongoing work of the Doctorate student Ing. M. Tapias. The laboratory developments mentioned in the lecture could not have been achieved without the intense involvement of the Geotechnical Laboratory staff: Prof. E. Romero, T. Pérez, J. Sánchez and V. Lozano. The help received from Lic. M. Obrador and R. Giménez during the preparation of the manuscript and figures is acknowledged with thanks. Part of the research reported has been financed by Research Projects awarded by the Spanish Ministry of Education.

References

Alonso, E.E. (2006) Field applications of unsaturated soil mechanics. Geotechnical Special Publication, v. 148, p. 1-33.

Alonso, E.E.; Gens, A. & Hight, D.W. (1987) Special Problem Soils. General Report. Proc. 9th European Conference on Soil Mechanics and Foundation Engineering. Dublin, v. 3, p. 1087-1146.

Alonso, E.E.; Gens, A. & Josa, A. (1990) A constitutive model for partially saturated soils, Géotechnique, v. 40:3, p. 405-430.

Alonso, E.E.; Olivella, S. & Pinyol, N.M. (2005) A review of Beliche Dam. Géotechnique, v. 55:4, p. 267-285.

Athanasiu, C.; Simonsen, A.S.; Soereide, O.K. & Tistel, J. (2005). Elastic and creep settlements of rock fills. Proc. 16th Int. Conf. Soil Mech. Geotech. Engng., Osaka, p. 1837-1843.

Cetin, H.; Laman, M. & Ertunç, A. (2000) Settlement and slaking problems in the world's fourth largest rock-fill dam, the Ataturk Dam in Turkey. Engineering Geology, v. 56:3-4, p. 225-242.

Charles, R.J. (1958) Static fatigue of glass. Journal of Applied Physics, v. 29, p. 1549-1560.

Charles, J.A. (1989). Geotechnical properties of coarse grained soils. Proc. of the 12th Int Conf on Soil Mechanics and Foundation Engineering, Rio de Janeiro, p. 2495-2519.

Charles, J.A. (1991). Laboratory compression tests and the deformation of rockfill structures. Advances in Rockfill Structures. NATO ASI Series E, v. 200, p. 73-95.

Charles, J.A. & Watts, K.S. (1980) The influence of confining pressure on the shear strength of compacted rockfill. Géotechnique, v. 4:3, p. 353-398.

Chávez, C. (2004) Estudio del Comportamiento Triaxial de Materiales Granulares de Tamaño Medio con Énfasis en la Influencia de la Succión. PhD Thesis, Universitat Politècnica de Catalunya. Barcelona, Spain.

Chávez, C.; Romero, E. & Alonso, E.E. (2009) A rockfill triaxial cell with suction control. Geotechnical Testing Journal, v. 32:3, p. 1-13.

Chávez, C. & Alonso, E.E. (2003) A constitutive model for crushed granular aggregates which include suction effects. Soils and Foundations, v. 43:4, p. 215-227.

Clements, R.P. (1981). The Deformation of Rockfill: Inter-Particle Behavior, Bulk Properties and Behavior in Dams. PhD. Thesis, Faculty of Engineering, King's College, London University.

Cundall, P.A. & Strack, O.D.L. (1979) A discrete numerical model for granular assemblies. Géotechnique 29:1, p. 47-65.

De Mello, V.F.B. (1977) Seventh Rankine Lecture: Reflections on design decisions of practical significance to embankment dams. Géotechnique, v. 27:3, p. 279-356.

Frossard, E. (2009) On the structural safety of large rockfill dams. Proc. 23rd Conf. on Large Dams. Q. 91-R. 39 Brasilia.

Frossard, E.; Hu, W.; Dano, C. & Hicher, P.-Y. (2012) Rockfill shear strength evaluation: a rational method based on size effects. Géotechnique, v. 62:5, p. 415-427.

Fumagalli, E. (1969) Tests on cohesionless materials for rockfill dams. J. Soil Mech. Found. Engng Div., v. 95(SM1), p. 313–330.

Gili, J.A. (1988) Modelo Microestructural para Medios Granulares No Saturados. PhD Thesis. Universitat Politècnica de Catalunya. Barcelona, Spain.

Gili, J.A. & Alonso, E.E. (2002) Microstructural deformation mechanisms of unsaturated granular soils. Int. J. Numer. Anal. Meth. Geomech., v. 26, p. 433-468.

Hardin, B.O. (1985) Crushing of soil particles. Jnl. of Geotech. Engng., v. 111:10, p. 1177-1192.

Justo, J.L. & Durand, P. (2000) Settlement-time behavior of granular embankments. Int. J. Numer. Anal. Methods Geomech., v. 24, p. 281-303.

Lee, D.M. (1992). The Angles of Friction of Granular Fills. Ph.D. dissertation, University of Cambridge.

Marachi, N.D.; Chan, C.K.; Seed, H.B. & Duncan, J.M. (1969) Strength and Deformation Characteristics of Rockfill Materials. Department of Civil Engineering. Report No. TE-69-5. University of California.

Marsal, R.J. (1973) Mechanical properties of rockfill. In: Embankment Dam Engineering. Casagrande. R.C. Hirschfeld & S.J. Poulos (eds) John Wiley & Sons, New York, p. 109-200.

Marsal, R.J.; Arellano, L.R.; Guzmán, M.A. & Adame, H. (1976) El Infiernillo: Behavior of Dams Built in Mexico. Instituto de Ingeniería, UNAM, Mexico.

McDowell, G.R. & Bolton, M.D. (1998) On the micromechanics of crushable aggregates. Géotechnique, v. 48:5, p. 667-679.

Mesri, G. & Castro, A. (1987). C_α/C_c concept and K_0 during secondary compression. J. Geotech. Engng, ASCE v. 113:3, p. 230-247.

Naylor, D.J.; Maranha das Neves, E.; Mattar, D. Jr. & Veiga Pinto, A.A. (1986) Prediction of construction performance of Beliche Dam. Géotechnique, v. 36:3, p. 359-376.

Naylor, D.J.; Maranha das Neves, E. & Veiga Pinto, A.A. (1997) A back-analysis of Beliche Dam. Géotechnique, v. 47:2, p. 221-233.

Nobari, E.S. & Duncan, J.M. (1972) Effect of Reservoir Filling on Stresses and Movements in Earth and Rockfill Dams. Department of Civil Engineering, Report No. TE-72-1. University of California.

Oldecop, L.A. & Alonso, E.E. (2001) A model for rockfill compressibility. Géotechnique, v. 51:2, p. 127-139.

Oldecop, L.A. & Alonso, E.E. (2003) Suction effects on rockfill compressibility. Géotechnique, v. 53:2, p. 289-292.

Oldecop, L.A. & Alonso, E.E. (2004) Testing rockfill under relative humidity control. Geotechnical Testing Journal, v. 27:3, p. 1-10.

Oldecop, L.A. & Alonso, E.E. (2007) Theoretical investigation of the time-dependent behavior of rockfill. Géotechnique, v. 57:3, p. 289-301.

Olivella, S.; Carrera, J.; Gens, A. & Alonso, E.E. (1994) Nonisothermal multiphase flow of brine and gas through saline media. Transport in Porous Media, v. 15, p. 271-293.

Olivella, S.; Gens, A.; Carrera, J. & Alonso, E.E. (1996) Numerical formulation for simulator (Code_Bright) for coupled analysis of saline media. Engineering Computations, v. 13:7, p. 87-112.

Ortega, E. (2008) Comportamiento de Materiales Granulares Gruesos. Efecto de la Succión. Ph.D. Thesis. Universitat Politècnica de Catalunya, Barcelona, Spain.

Poorooshasb, H.; Holubec, I. & Sherbourne, A. (1966) Yielding and flow of sand in triaxial compression. Part I. Canadian Geotech. Jnl., v. 3:4, p. 179-190.

Ramon, A.; Alonso, E.E. & Romero, E.E. (2008) Grain size effects on rockfill constitutive behavior. Proc. of the 1st European Conf. on Unsaturated Soils. Taylor & Francis, p. 341-347.

Russell, A.R. & Wood, D.M. (2009) Point load tests and strength measurements for brittle spheres. International Journal of Rock Mechanics & Mining Sciences v. 46, p. 272- 280

Schnitter, N.J. (1994) A History of Dams. The Useful Pyramids. Balkema, Rotterdam.

Sherard, J.L. & Cooke, J.B. (1987). Concrete-face rockfill dam: I. Assessment. J. Geotech. Engng ASCE, v. 113:10, p. 1096-1112.

Soriano, A. & Sánchez, F.J. (1999) Settlements of railroad high embankments. Proc. 12th European Conf. on Soil Mech. and Geotech. Eng., Amsterdam, The Netherlands, p. 1885-1890.

Sowers, G.F.; Williams, R.C. & Wallace, T.S. (1965) Compressibility of broken rock and settlement of rockfills. Proc. 6th Int. Conf. on Soil Mech. & Found. Engng. Montreal, Canada, p. 561-565.

Terzaghi, K. (1960) Discussion on salt springs and lower bear riverdams. Transportations, v. 125:2, p. 139-148.

Veiga Pinto, A.A. (1983) Previsao do Comportamento Estrutural de Barragens de Enrocamento. Ph.D. Thesis, Laboratorio Nacional de Engenharia Civil, Lisbon.